doi:10.1093/brain/aws270 Brain 2012: 135; 3265–3281 | 3265

BRAIN
A JOURNAL OF NEUROLOGY

Back seat driving: hindlimb corticospinal neurons assume forelimb control following ischaemic stroke

Michelle Louise Starkey,[1,*] Christiane Bleul,[1] Björn Zörner,[1,†] Nicolas Thomas Lindau,[1] Thomas Mueggler,[2,‡] Markus Rudin[2] and Martin Ernst Schwab[1]

1 Department of Health Sciences and Technology, Brain Research Institute, University of Zurich, 8057 Zurich, Switzerland
2 Animal Imaging Centre, ETH Zurich, 8093 Zurich, Switzerland

*Present address: Balgrist University Hospital, Forchstrasse 340, 8008 Zurich, Switzerland
†Present address: Neurology Clinic, University Hospital Zurich, Frauenklinikstrasse 26, 8091 Zürich, Switzerland
‡Present address: Neuroscience Department, Pharmaceutical Division, F. Hoffmann-La Roche Ltd, 4070 Basel, Switzerland

Correspondence to: Michelle L. Starkey, PhD,
Balgrist University Hospital,
Forchstrasse 340,
CH-8008 Zurich,
Switzerland
E-mail: mstarkey@paralab.balgrist.ch

Whereas large injuries to the brain lead to considerable irreversible functional impairments, smaller strokes or traumatic lesions are often associated with good recovery. This recovery occurs spontaneously, and there is ample evidence from preclinical studies to suggest that adjacent undamaged areas (also known as peri-infarct regions) of the cortex 'take over' control of the disrupted functions. In rodents, sprouting of axons and dendrites has been observed in this region following stroke, while reduced inhibition from horizontal or callosal connections, or plastic changes in subcortical connections, could also occur. The exact mechanisms underlying functional recovery after small- to medium-sized strokes remain undetermined but are of utmost importance for understanding the human situation and for designing effective treatments and rehabilitation strategies. In the present study, we selectively destroyed large parts of the forelimb motor and premotor cortex of adult rats with an ischaemic injury. A behavioural test requiring highly skilled, cortically controlled forelimb movements showed that some animals recovered well from this lesion whereas others did not. To investigate the reasons behind these differences, we used anterograde and retrograde tracing techniques and intracortical microstimulation. Retrograde tracing from the cervical spinal cord showed a correlation between the number of cervically projecting corticospinal neurons present in the hindlimb sensory–motor cortex and good behavioural recovery. Anterograde tracing from the hindlimb sensory–motor cortex also showed a positive correlation between the degree of functional recovery and the sprouting of neurons from this region into the cervical spinal cord. Finally, intracortical microstimulation confirmed the positive correlation between rewiring of the hindlimb sensory–motor cortex and the degree of forelimb motor recovery. In conclusion, these experiments suggest that following stroke to the forelimb motor cortex, cells in the hindlimb sensory–motor area reorganize and become functionally connected to the cervical spinal cord. These new connections, probably in collaboration with surviving forelimb neurons and more complex indirect connections via the brain-stem, play an important role for the recovery of cortically controlled behaviours like skilled forelimb reaching.

Keywords: stroke; functional recovery; plasticity; sprouting; movement control
Abbreviations: CST = corticospinal tract; ICMS = intracortical microstimulation

Received March 2, 2012. Revised July 17, 2012. Accepted August 12, 2012

Introduction

Small cortical stroke lesions are often followed by good recovery of function both experimentally and clinically. Under specific circumstances, the adult cortex is considerably plastic after a lesion, and there is clinical and preclinical evidence that following small, subtotal lesions to the cortex, adjacent undamaged areas 'take over' control of lost or disrupted functions (Feydy *et al.*, 2002; Werhahn *et al.*, 2003; Murphy and Corbett, 2009; Dancause and Nudo, 2011). However, the exact mechanisms behind this phenomenon are unknown. Following small subtotal strokes, the cortical area surrounding the stroke lesion, the peri-infarct region, has many properties that could aid growth and functional recovery, such as changes in gene expression, e.g. of cytoskeletal proteins, the growth-associated protein GAP-43 and neurotrophic factors (Stroemer *et al.*, 1993; Keyvani *et al.*, 2002; Lu *et al.*, 2003; Li and Carmichael, 2006; Li *et al.*, 2010). Additionally, under these circumstances, regions directly surrounding the peri-infarct area have been shown to remain relatively damage free and functional (Enright *et al.*, 2007; Zhang and Murphy, 2007; Winship and Murphy, 2008; Brown *et al.*, 2009) and thus are potentially available for processes of recovery. Sprouting of neurites and changes in dendritic spine densities in this area have been shown preclinically (Zhang *et al.*, 2005; Brown *et al.*, 2007, 2010; Li *et al.*, 2010). The situation is different following large cortical lesions, for example, those that involve the entire motor cortex (unilaterally). In animal models, cortical map shifts following such lesions are often permanent, i.e. activation shifts to the non-impaired cortex (Emerick *et al.*, 2003; Markus *et al.*, 2005), whereas in humans, such map shifts tend to be transitory and activations shift back to the damaged cortex as functional recovery progresses (Liepert *et al.*, 2000; Marshall *et al.*, 2000).

Functionally, the ipsilesional cortex has been shown to be highly active post-lesion such that representations of the damaged body parts relocate to surrounding undamaged (peri-infarct) tissue both clinically and preclinically. For example, following lesion to the forelimb motor cortex in adult rats, it was shown that partial recovery of forelimb function was associated with a reduction of contralesional functional MRI responses in favour of significant responses in the infarct periphery on the ipsilesional side (Dijkhuizen *et al.*, 2001, 2003). In humans, it was shown that after stroke, an enlargement of the hand region of the ipsilesional cortex was correlated with improved arm/hand movement control and clinical scores (Cicinelli *et al.*, 1997; Traversa *et al.*, 1997; Ward *et al.*, 2006, 2007). Also, following rehabilitative training in chronic stroke patients, a shift in the motor output maps to an area adjacent to the lesion was observed (Liepert *et al.*, 1998; Marshall *et al.*, 2000). In most of these functional studies, however, the exact mechanisms behind these changes remain elusive. Activity changes in specific cortical areas may result from a reduction in inhibition from horizontal or callosal connections (Adesnik and Scanziani, 2010). Alternatively, new connections may form due to lesion-induced sprouting at the cortical or subcortical level (Kaas *et al.*, 2008; Li *et al.*, 2010). Here we show that following an ischaemic subtotal lesion of the rat forelimb motor cortex, spontaneous recovery of forelimb function was correlated with hindlimb corticospinal neurons changing their target, anatomically and functionally, to the cervical, forelimb-related, spinal cord. These results in rodents have potential implications for understanding the anatomical basis of recovery from small subtotal strokes in humans.

Materials and methods

Animals

Adult female Long-Evans rats (200–250 g, $n = 170$) were obtained from a specific pathogen-free breeding colony (Charles River). Animals were kept in groups of four in standardized cages (Type 4 Macrolon) on a standard regimen of 12-h light/dark cycle with food and water *ad libitum*. All experiments were performed in accordance with the guidelines of the Veterinary Office of the Canton Zurich, Switzerland.

Behavioural training and testing

The single pellet grasping test (Whishaw and Pellis, 1990; Whishaw *et al.*, 1993; Starkey *et al.*, 2011) assesses fine motor control of the forelimb. Animals were placed in a Plexiglas box (34 × 14 cm) with two openings on opposite ends. During a training session, rats had to grasp 25 sugar pellets (45-mg dustless precision pellets, TSE Systems Intl. Group) presented at alternating ends. Animals were given five practice pellets followed by 20 test pellets. A maximum time of 10 min was given to grasp all pellets. Grasping performance was scored by the experimenter blinded to the group as follows: a trial, defined as the animal putting its paw through the grasping window to grasp a new pellet presented to the preferred side into a shallow well, was scored as 1 (successful grasp) if the animal retrieved the pellet with its impaired paw and brought it directly to its mouth. A score of 1 was given either if the animal succeeded on first attempt or if it used several attempts to grasp the pellet, without retracting the paw through the window and into the box, which was defined as the end of the attempt. If the animal succeeded in grasping the pellet but dropped it inside the box before bringing it to its mouth, the trial was scored as 0.5. If the animal knocked the pellet off the small shallow well on the shelf without retrieving it, the trial was scored as 0. The success rate was calculated as the sum of the retrieved pellets divided by the number of trials. Owing to variations in the abilities of animals to learn this complicated behavioural task, all of our success rates are expressed as a percentage of the baseline score, thus all animals achieved 100% at baseline. Animals were trained for ~3 weeks before baseline recordings and were food deprived the night before training and testing sessions. Only animals with a 60% or higher success rate (prior to normalization) at baseline were selected for the study.

Post-lesion animals were tested on Days 2, 4, 7, 14, 21, 28, 35 and 42 by an experimenter blinded to the treatment and recovery group. All animals that scored a success rate ⩾60% of baseline on Day 2 were excluded from the study, as it was assumed that they had not sustained an adequate lesion (59 of 170 lesioned animals were excluded for this reason). In addition, each testing session was filmed (Panasonic NVGS500, 25 frames/s), and single grasps were evaluated using frame-by-frame video analysis (Virtualdub; www.virtualdub.org) as described in detail previously (Starkey *et al.*, 2011). Briefly, five successful grasps were analysed under the following criteria: body position, targeting, number of attempts, pellet position,

supination, pellet sensing and pellet release (Starkey *et al.*, 2011). Each subcategory contained scores to categorize the movement components. For the purpose of the present data, we found that first attempt success and body position in relation to the pellet was important. If the animal grasped the pellet at the first attempt it scored 1, if subsequent attempts were required (without the animal retracting its paw back through the grasping window), regardless of number, the animal scored 2. Several attempts meant that the animal grasped several times when its paw was already through the grasping window. If the animal brought its paw back into the box without having grasped the pellet and then started grasping again and was successful then this would be scored as a failed attempt followed by a successful attempt. For body position, the most perfect body position, meaning the animal was standing directly in front of the pellet, was scored 1. For a full description of the analysis see Starkey *et al.* (2011).

Endothelin-1 lesion to the forelimb motor area

Endothelin-1 lesions were performed similarly to those described previously (Gilmour *et al.*, 2004; Zhang *et al.*, 2005; Hewlett and Corbett, 2006; Zorner *et al.*, 2010). Trained animals ($n = 170$) from the retrograde acute/chronic, anterograde acute/chronic and intracortical microstimulation (ICMS) chronic groups were anaesthetized with a subcutaneous injection of a mixture of hypnorm/dormicum (hypnorm: 120 µl/200 g body weight, Janssen Pharmaceutics; dormicum: 0.75 mg/200 g body weight, Roche Pharmaceuticals). The animal was fixed into a stereotaxic frame, the scalp was opened and the skull cleaned. The lesion area (forelimb motor cortex area of the preferred paw as determined with the single pellet reaching test) was marked based on stereotaxic coordinates defined by retrograde tracing (Supplementary Fig. 1A–F and H). The skull in this area was drilled (Foredom Electric Co.) at the slowest drill speed and intermittently cooled with Ringer's solution (Fresenius Kabi) until only a thin veneer of bone remained. This veneer of bone was then carefully removed. Stereotaxic injections of endothelin-1 (0.3 µg/µl, American Peptide Company) using a 10 µl syringe (World Precision Instruments) driven by an electric pump (World Precision Instruments) with a flow rate of 3 nl/s were made through an intact dura. Injections were 1×300 nl in the rostral forelimb area and 7×150 nl in all caudal forelimb area sites. Site 1 (rostral forelimb area): anterior/posterior = + 3.5 mm, mediolateral = 2.0 mm, dorsoventral = −1.5 mm; Site 2 (caudal forelimb area): anterior/posterior = + 0.5 mm, mediolateral = 2.0 mm, dorsoventral = −1.0 mm; Site 3 (caudal forelimb area): anterior/posterior = + 1.5 mm, mediolateral = 2.0 mm, dorsoventral = −1.0 mm; Site 4 (caudal forelimb area): anterior/posterior = + 1.5 mm, mediolateral = 3.0 mm, dorsoventral = −1.0 mm; Site 5 (caudal forelimb area): anterior/posterior = + 0.5 mm, mediolateral = 3.0 mm, dorsoventral = −1.0 mm; Site 6 (caudal forelimb area): anterior/posterior = + 1.0 mm, mediolateral = 2.5 mm, dorsoventral = −1.0 mm; Site 7 (caudal forelimb area): anterior/posterior = + 0.5 mm, mediolateral = 3.5 mm, dorsoventral = −1.0 mm; Site 8 (caudal forelimb area): anterior/posterior = + 1.5 mm, mediolateral = 3.5 mm, dorsoventral = −1.0 mm. Thus, a total of 1.35 µl endothelin-1 was injected into the forelimb area. There was a 3-min waiting time after each injection and 10 min after the last injection. The waiting time was required to limit the backflow of the endothelin-1 out of the brain. Previous publications (Adkins *et al.*, 2004) have reported that the animal should remain unmoved for at least 5 min after the injections, which is why there was a longer waiting time given after the final injection. Sham animals ($n = 8$) received the entire surgery including the needle penetration but excluding the injection of endothelin-1. At the end of the surgery, the animal was removed from the frame and sutured. The animals were warmed on a heating pad for 24 h before being returned to their home room. Immediately after surgery and for up to 3 days post-lesion, rats received subcutaneous injections of an analgesic (Rimadyl®, 2.5 mg per kg body weight, Pfizer), an antibiotic (Baytril®, 5 mg per kg body weight, Bayer) and saline (Ringer's solution, 5 ml, glucose 5%, NaCl 0.9% 2:1, Fresenius Kabi). The health of the animals was checked daily for the duration of the experiment.

Assessment of lesion by magnetic resonance imaging

In vivo MRI examinations of the brain were performed on a 4.7-T Pharmascan magnetic resonance system 47/16 (Bruker BioSpin) equipped with a birdcage resonator of 24-mm diameter 24 h post-lesion on a subset of lesioned and sham-operated animals ($n = 24$, Supplementary Fig. 1G) to check that the lesions were reproducible. Animals were anaesthetized with isoflurane supplied in an air/oxygen mixture (3/1) at 4% for induction and 1.8% for maintenance. T_2-weighted images were acquired using a 3D fast spin echo rapid acquisition with relaxation enhancement (Hennig *et al.*, 1986) sequence with a repetition time of 1500 ms, an inter-echo time of 6.5 ms and a train of 16 echoes (no averaging) leading to an echo time of 54.6 ms, field of view of $40 \times 35 \times 16.8$ mm^3 and a matrix of $256 \times 225 \times 56$ and a voxel dimension of $0.156 \times 0.156 \times 0.3$ mm^3. For image acquisition, rats were placed on a support where body temperature was maintained at 37°C using warm air. The total MRI scanning time was 30 min per rat. To export the data into the analysis software (ImageJ, Version 1.37 c, National Institutes of Health), sagittal and coronal images were re-sliced using the ParaVision® (Bruker, BioSpin) software tool Jive.

Intracortical microstimulation

Six weeks post-lesion a subset of trained, lesioned ($n = 8$) and trained, normal control ($n = 8$, Supplementary Fig. 1G) rats were anaesthetized with an intramuscular injection of a mixture of ketamine (50 mg/ml, 70 mg/kg body weight, Streuli Pharma) and xylazine (20 mg/ml, 5 mg/kg body weight, Streuli Pharma). It took a short time (<3 h) to map the entire hindlimb sensory–motor area with ICMS in these animals; therefore, supplementary doses of anaesthetic were rarely required. On the few occasions where additional anaesthetic was required, supplementary intramuscular doses of ketamine (50 mg/ml, 20 mg/kg body weight) were given to maintain the animal at an anaesthetic level that was unresponsive to paw pinch, as described previously (Neafsey *et al.*, 1986; Z'Graggen *et al.*, 2000; Emerick *et al.*, 2003). Following the supplementary dose of ketamine, ICMS did not restart until the same response (visually and with EMG) was seen in the same location with the identical current as was observed in the final two points before the injection. The fore- and hindlimbs were shaved (to better visualize muscle movements), and the animal was secured in a stereotaxtic frame. Mannitol (20%, 17 ml/kg, B. Braun Medical) was delivered subcutaneously to reduce swelling of the cortex. The ipsilesional motor cortex was marked (based on stereotaxic coordinates defined by retrograde tracing). A craniotomy was performed as described earlier for the lesion but instead over the ipsilesional hindlimb sensorimotor cortex. The dura was kept intact, and warm saline or mineral oil was used to keep the brain moist. Using Bregma as a landmark, electrode penetrations perpendicular to the pial surface were made on a grid in random sequence. This grid covered

the entire hindlimb sensory–motor area and the caudal parts of the forelimb area up to the lesion site (anterior/posterior = +0.8 mm to −2.4 mm, mediolateral = 1 mm to 3.2 mm, depths from 1.3–1.9 mm). Stimulation points were a minimum of 400 μm apart. A glass-insulated platinum/tungsten stimulation electrode with an impedance of 1–2 MΩ (Thomas Recording) was used to map the cortex. Stimulation was performed with 45 ms trains of 0.2 ms biphasic pulses at 333 Hz. For the readout, visually detectable movements and EMG of the fore- and hindlimb were used. EMG recordings were performed for muscle groups (forelimb: trapezius for shoulder movement, biceps and triceps for elbow, extensor digitorum for wrist and finger; hindlimb: soleus and tibialis for general hindlimb movements). The signals were amplified, filtered, digitized and visualized with PowerLab (ADInstruments). One investigator (blinded to the treatment groups and the location of the electrode) applied the stimulation current and assessed the EMG output, while the other experimenter (also blinded to the treatment and recovery groups, as well as the current applied) assessed the limb movements. Stimulation was considered successful if a visible movement and/or an EMG response could be observed at a stimulation current $\leqslant$90 μA. The current threshold for every point on the cortex was determined as the lowest current necessary to elicit a consistent response, either forelimb, hindlimb or for the forelimb and then hindlimb when both responded at a particular point. When no response was seen at the maximal current (90 μA) at any depth, 'no response' was recorded. In the case of both fore- and hindlimbs responding, the threshold current was defined for the forelimb first and then the hindlimb. Thus, a forelimb/hindlimb response meant that responses for the fore- and hindlimb were found at the same map point but not necessarily at the same depth or current. The maximal current (90 μA) was chosen based on previous publications (Neafsey and Sievert, 1982; Gharbawie *et al.*, 2005; Brus-Ramer *et al.*, 2007) where a maximal current of 100 μA was used. EMG data were high and low pass filtered (10–500 Hz), and a notch filter (45–55 Hz) was applied. At the end of the ICMS session the animal was removed from the frame, sutured and warmed on a heating pad for 24 h before being returned to their home room.

For the ICMS group, the area of the brain eliciting forelimb movements was measured following the construction of the ICMS maps. For this the full maps were loaded into Image J (Version 1.42, National Institutes of Health). The area where both fore- and hindlimb responses were elicited was measured, i.e. the area containing red dots (Fig. 5A and D) as a percentage of double responses in the hindlimb area, which was measured in the same way by outlining, in this case, the yellow and red dots (Fig. 5A and D).

Retrograde tracing: cervical spinal cord (forelimb)

Following the completion of behavioural testing, the sham group (n = 8, Supplementary Fig. 1G), the retrograde tracing (acute and chronic) groups (n = 20, Supplementary Fig. 1G) and double-labelling (control and chronic) groups (n = 8, Supplementary Fig. 1G) received retrograde tracer injections into the cervical spinal cord (Supplementary Fig. 1A–F). Animals were anaesthetized as mentioned previously for the lesion surgery, and a laminectomy was performed at vertebral level C5–C6 (spinal level C6–C7). The animal was then attached to a stereotaxic frame at vertebral levels C2 and T2. Fast blue retrograde tracer (2% suspension in 0.1 M phosphate buffer with 2% dimethyl sulphoxide, EMS-Chemie) was injected stereotaxically using a 28 gauge, 10 μl syringe (Hamilton, BGB Analytik) driven by an electric pump (World Precision Instruments) with a flow rate of 170 nl/s (Supplementary Fig. 1A and B). Six injections of 120 nl each were made unilaterally into the cervical spinal cord ventral horn, contralateral to the lesioned cortex. The injection coordinates were as follows: 0.8 mm lateral to the midline and 1.2 mm below the spinal cord surface. The first injection was made at the C6 level. When this was complete, the injection needle was retracted, moved rostrally by 0.8 mm, and the second injection was then made. This method was repeated, moving 0.8 mm rostral for each subsequent injection until all six injections had been made. The application needle was kept in place for 3 min after each injection. After the last injection, the animals (sham and acute and chronic retrograde groups) either received postoperational care (see later in the article) or had their hindlimb sensory–motor connections traced in addition (double retrograde groups, see later in the article). At the end of the surgery, the animal was removed from the frame and sutured. The animals were warmed on a heating pad for 24 h before being returned to their home room. Immediately after surgery and for up to 3 days post-lesion, rats received subcutaneous injections of an analgesic (Rimadyl®, 2.5 mg per kg body weight, Pfizer), an antibiotic (Baytril®, 5 mg per kg body weight, Bayer) and saline (Ringer's solution, 5 ml, glucose 5%, NaCl 0.9% 2:1, Fresenius Kabi). The health of the animals was checked daily for the entire experiment.

Retrograde tracing: lumbar spinal cord (hindlimb)

Under the same anaesthesia as mentioned earlier, animals from the double-labelling group (control and chronic) (n = 8, Supplementary Fig. 1G) received retrograde tracing of their hindlimb-projecting corticospinal tract (CST). A second laminectomy was performed at lumbar levels T12–T13 (spinal level L1–L3), and the animal was attached to the stereotaxic frame at vertebral level T13. The lumbar spinal cord segments L1–L3 were injected with tetramethylrhodamine (10% in injectable water, Invitrogen) using a 28 gauge, 10 μl syringe driven by an electric pump with a flow rate of 170 nl/s (Supplementary Fig. 1A and C). Six injections of 120 nl each were made of the tracer unilaterally into the lumbar spinal cord ventral horn with the injection coordinates 0.7 mm lateral to the midline and 1 mm below the spinal cord surface. After the last injection, the animal was sutured and kept on a heating pad for 24 h to recover before being returned to their home room. As mentioned earlier, they were given postoperational care for up to 3 days post-lesion and then were checked daily. This constituted: subcutaneous injections of an analgesic (Rimadyl®, 2.5 mg per kg body weight, Pfizer), an antibiotic (Baytril®, 5 mg per kg body weight, Bayer) and saline (Ringer's solution, 5 ml, glucose 5%, NaCl 0.9% 2:1, Fresenius Kabi).

Additionally, before the start of the experiment in order to establish lesion coordinates, the motor cortex was mapped with lumbar and cervical retrograde tracing in normal control, trained animals (mapping group, n = 10, Supplementary Fig. 1G). For these animals, following a subcutaneous injection of hypnorm/dormicum (as mentioned earlier), the two laminectomies were performed as described earlier. The cervical spinal cord was traced with Fast blue (as mentioned earlier) and the lumbar spinal cord with diamidino yellow dihydrochloride, 2% suspension in 0.1 M phosphate buffer and 2% dimethyl sulphoxide (Sigma-Aldrich), using the same protocol as described earlier for tetramethylrhodamine. It was not possible to use diamidino yellow dihydrochloride for the entire experiment because it went out of production before the double-labelling experiments were performed. However, we carried out pilot experiments in the laboratory which

showed that tetramethylrhodamine had a comparable efficiency to diamidino yellow dihydrochloride (data not shown).

For all these surgeries, the tracers were always injected unilaterally on the side to label the cortex of the preferred paw as determined behaviourally (Supplementary Fig. 1B and C). Post-mortem all tracer injection sites were examined in detail. Animals where any of the injections hit either the main portion of the CST in the dorsal funiculus or where spill over to the opposite side of the spinal cord had occurred were excluded from the study (22 of the total 170 animals were excluded because of this problem). Fast blue tracing of the cervical spinal cord labelled layer V pyramidal cells in both the rostral (Supplementary Fig. 1D) and caudal (Supplementary Fig. 1E) forelimb areas. Tetramethylrhodamine tracing of the lumbar spinal cord labelled layer V pyramidal cells in the hindlimb sensory–motor area exclusively (Supplementary Fig. 1F). We chose Fast blue because it is known to be a highly efficient tracer, which was confirmed before the start of the experiment. This tracer labels neurons even when at low local concentration or low levels of sprouting. This was confirmed by the low variation between the numbers of cells labelled in normal control animals 10 670 ± 1190 (SEM) cells.

The locations of the labelled cells were reconstructed in 3D (see later in the article) to map the fore- and hindlimb sensory–motor cortices. Fixation of the brain before 3D reconstruction was done by perfusion (described later in the article). Shrinkage of the brains during this process, which could have affected the coordinates chosen for the lesion, was very minor. This minor shrinkage was compensated for by freezing the brains rapidly, simultaneously and identically between all groups. Finally, all animals were tested for lesion deficit and excluded if the lesion was not considerable. Along with the positions of each cell, we also labelled Bregma on each of the 2D representations of the 3D reconstructions. Therefore, following reconstruction of the mapping animals, we were able to accurately overlay all of the reconstructions using Bregma as the landmark (Supplementary Fig. 1H). This gave an 'average' hindlimb area, i.e. the region where hindlimb-projecting cells were found in all animals, i.e. the darkest yellow region (Supplementary Fig. 1H). For analysis, we selected this as our hindlimb area (appears as shaded yellow area on other reconstructions). Thus, it is highly likely that for each animal we underestimate the actual number of cells in this region.

Anterograde tracing of hindlimb corticospinal tract

In another group of animals, following the completion of behavioural testing, trained and lesioned animals (acute and chronic anterograde groups, $n = 27$, Supplementary Fig. 1G) were anaesthetized as described earlier. The animal was fixed into a stereotaxic frame, the scalp was opened and the skull cleaned. The hindlimb sensory–motor area was marked according to stereotaxic coordinates defined in the mapping experiments detailed earlier. A craniotomy was performed (as mentioned earlier) over the ipsilesional hindlimb sensory–motor area. Stereotaxic injections of the anterograde tracer biotinylated dextran amine (10 000 molecular weight, 10% solution in 0.01 M PBS, Invitrogen) were made through an intact dura using a 35 gauge, 10 µl syringe (World Precision Instruments) driven by an electric pump (World Precision Instruments) with a flow rate of 6 nl/s. A total volume of 400 nl was injected at two injection sites (200 nl per site). The injection coordinates were Site 1: anterior/posterior = −1.5 mm, mediolateral = 2.5 mm; Site 2: anterior/posterior = −2.5 mm, mediolateral = 2.5 mm. All injections were at 1 mm depth, and the syringe remained in place for 2 min after completion of each injection. After the second injection, the rat was carefully removed from the frame and sutured and given postoperational care (see above). The animals were warmed on a heating pad for 24 h before being returned to their home room, and their health was checked daily for the remainder of the experiment.

Tissue preparation and staining

One week after retrograde tracing (Fast blue, tetramethylrhodamine, diamidino yellow dihydrochloride) and 3 weeks after anterograde tracing (biotinylated dextran amine), animals were deeply anaesthetized with pentobarbital (450 mg/kg body weight i.p.; Abbott Laboratories), and perfused transcardially with 100 ml Ringer's solution (containing 100 000 IU/l heparin, Liquemin, Roche, and 0.25% $NaNO_2$) followed by 300 ml of 4% phosphate-buffered paraformaldehyde (pH 7.4). Spinal cords and brains were dissected and post-fixed in the same fixative overnight at 4°C before being cryoprotected in phosphate-buffered 30% sucrose for an additional 5 days. The cervical spinal cord (C1–T1), lumbar spinal cord (L1–L5), brain and brainstem were embedded in Tissue-Tec (OCT) and frozen in isopentane (Sigma) at −40°C. Brains and spinal cords of retrogradely traced animals were cut in 40-µm-thick coronal sections on a cryostat and collected on slides (Superfrost) before being cover-slipped with Mowiol® mounting medium (Calbiochem). Biotinylated dextran amine-traced spinal cords were cut in 50-µm thick horizontal sections, and the brainstems from the same animals (for normalization of tracing) were cut in 50-µm thick coronal sections on a cryostat and collected on slides (Superfrost) before being stained by on-slide processing using the nickel-enhanced DAB (3,3′-diaminobenzidine) protocol (Vectastain® ABC Elite Kit, Vector Laboratories; 1:100 in Tris-buffered saline plus Triton™ X-100) as described previously (Herzog and Brosamle, 1997).

Quantification of hindlimb corticospinal tract collaterals in the cervical spinal cord

Collaterals branching off the main CST labelled from the hindlimb sensory–motor cortex in the cervical spinal cord were counted in all biotinylated dextran amine-traced animals (acute and chronic anterograde groups, $n = 27$, Supplementary Fig. 1G). In horizontal sections of the spinal cord segments C1–T1 'stem' collaterals were counted at the white/grey matter interface by an experimenter blinded to the group at a final magnification of × 200. To correct for variations in biotinylated dextran amine uptake, we normalized the quantitative data by counting biotinylated dextran amine-labelled axons in the brainstem in three rectangular areas (200 μm^2) per slide on three sections per animal. Results are expressed as a collateralization index, calculated as the mean of the total number of 'stem' collaterals in the cervical spinal cord divided by the average of labelled hindlimb CST fibres per 200 μm^2 in the brainstem in sections from the main pyramidal tract at the level of the brainstem (facial nerve).

Three dimensional reconstruction of lesion and fore- and hindlimb corticospinal tract neuron position in the cortex

Retrogradely labelled cells (Fast blue, tetramethylrhodamine, diamidino yellow dihydrochloride) of all retrogradely traced animals remaining in

the study after inspection of the injection sites (sham, retrograde acute/chronic, ICMS control/chronic, double labelling control/chronic, and mapping groups, $n = 62$, Supplementary Fig. 1G) and the lesion sites of all lesioned animals (retrograde acute/chronic, anterograde acute/chronic, double-labelling control/chronic, ICMS control/chronic, $n = 71$, Supplementary Fig. 1G) were reconstructed in 3D by an experimenter blinded to the treatment groups using Neurolucida 8.0 (MicroBrightField). Every ninth section and thus cells present at 360 μm intervals were reconstructed in series to give a 3D image of the brain. Data shown are dorsal views of full 3D reconstructions (2D representations), total lesion volume, total Fast blue labelled/forelimb projecting cells on the ipsi- and contralesional cortex, total diamidino yellow dihydrochloride/tetramethylrhodamine labelled/hindlimb projecting cells on the ipsi- and contralesional cortex, and double-labelled/fore- and hindlimb projecting cells on the ipsilesional cortex. As only every ninth section was reconstructed, the final cell counts were multiplied by nine to give an extrapolated final cell count. However, 2D representations of the 3D reconstructions show every ninth section, and thus under-represent the total number of labelled cells. In order to reconstruct the lesion site, alternate sections from all lesioned animals were stained with cresyl violet. These sections were also reconstructed, and the lesioned area was superimposed (red shaded area) onto the corresponding 2D representations of the 3D reconstructions of the retrogradely traced cells. To define the medial and lateral caudal forelimb area, a line was drawn rostro-caudally along the lateral edge of the hindlimb area on every brain. This line transected the caudal forelimb area dividing it into a medial and lateral part within which the Fast blue-labelled cells were counted. In order for comparisons to be made, all reconstructions are shown with the lesion and ipsilesional (contralateral) tracing on the right side. As animals received lesions impairing their preferred paw, 2D representations of the 3D reconstructions were flipped wherever necessary.

For lesioned, retrogradely traced animals ($n = 20$, Supplementary Fig. 1G), the hindlimb sensory–motor areas were defined by overlaying the reconstructed hindlimb sensory–motor areas of the retrogradely traced mapping animals ($n = 10$, Supplementary Fig. 1G) using Neurolucida 8.0. For this we traced around the hindlimb areas with ImageJ. The area where all hindlimb areas overlapped (darkest yellow area in Supplementary Fig. 1H, outlined in yellow) was defined as the averaged hindlimb sensory–motor area. This averaged hindlimb sensory–motor area was then superimposed on all reconstructions from lesioned animals using defined landmarks. In the control and chronic ICMS and control and chronic double-labelling groups, all traced cells, including the hindlimb sensory–motor cells, were mapped.

Defining recovery groups

The animals showed a high degree of variability in their recovery profiles following injury (Fig. 1E). Owing to this variability, we decided to show data for single animals instead of group averages. We decided to average the score that the animals achieved at Days 35 and 42 because by this time point the animals were no longer improving in function, but there was variability in their actual scores, as has been reported previously (Whishaw, 2000). Therefore, we took the average of these two time points to give a more accurate score due to the inherent variability in this task, which is never completely stable as it depends on a number of factors in addition to function such as: motivation, attention and slight changes in the experimental room. To define 'good' and 'bad' recovery groups, the percentage change in success rate on the single pellet reaching task between Days 2 and 35/42 was calculated. All animals where the percentage change was $>50\%$ were put into the good recovery group. The range of percentage changes in this group was 51.8–93.2%. Whereas, all animals where the percentage was $<50\%$ were put into the bad recovery group. The range of percentage changes in this group was: -16.7% to 48.5%, plotted in addition to single animals scores (Fig. 1E) and number of hindlimb collaterals in the cervical spinal cord (Fig. 3H). In addition to this and for all other results, we carried out correlations between the measured variable (cell or fibre counts, volume of forelimb area) with the success rate at Day 35/42 for all the individual animals.

Statistical analysis

Grasping data were analysed using either parametric analysis of variance (two-/one-way repeated measures ANOVA) of the appropriate design, followed by Bonferroni *post hoc* pair-wise comparisons whenever a main effect or interaction achieved statistical significance; non-parametric (Mann–Whitney) tests; and Spearman or Pearson correlations between the behavioural recovery and the lesion volume, retrogradely labelled cells, anterogradely labelled fibres and ICMS data. All statistical analyses were conducted using the software Graph Pad Prism. Data are presented as means ± SEM, single data points represent single animals, and asterisks indicate significances: $*P \leqslant 0.05$, $**P \leqslant 0.01$, $***P \leqslant 0.001$.

Results

With a total of nine stereotaxic intracortical injections of endothelin-1, we achieved a considerable ischaemic destruction of the rostral (Fig. 1C) and caudal (Fig. 1B and D) forelimb motor cortex. In a subset of animals, T_2-weighted MRI scans 24 h post-lesion showed that the damage extended through all layers of the cortex (Fig. 1B), whereas sham lesioned animals showed no damage (Fig. 1A). Retrograde tracings from the cervical spinal cord segments C6 and C7 showed that $>70\%$ of the CST neurons innervating the forepaw-related spinal cord were destroyed (sham: 6233.6 ± 798.4 Fast blue-labelled cells in forelimb area; chronic lesioned: 1823.6 ± 312.2 Fast blue-labelled cells in forelimb area). However, small numbers of neurons remained, mostly in the rostral forelimb area and the lateral sensory areas (Table 1 and Fig. 2A–D).

Skilled reaching for single pellets through a small slit in a Plexiglas box was used, as it is a well-established test for CST-dependent forelimb function. Most animals showed a 60–80% deficit in success rate at Day 2 post-lesion. Lesion positions were variable between animals (Fig. 2D), but this was not correlated to initial lesion deficit, which was large in all cases. Those that achieved a superior performance at Day 2 were excluded from further analysis (59 of the original 170 animals lesioned were excluded for this reason), as they had not received a sufficient lesion to the forelimb area to assess recovery. Over Days 14 to 35/42, the individual lesioned animals showed large differences in the recovery of digit and forelimb control as assessed in the single pellet grasping task (Fig. 1E). However, the majority of the rats showed good recovery of the original behaviour (change in the success rate between Day 2 and 35/42 $>50\%$; Fig. 1E), whereas the remainder of the animals showed poor recovery (change in the success rate between Day 2 and 35/42 $<50\%$; Fig. 1E). Interestingly, there was no significant correlation between behavioural recovery and the overall lesion volume as determined

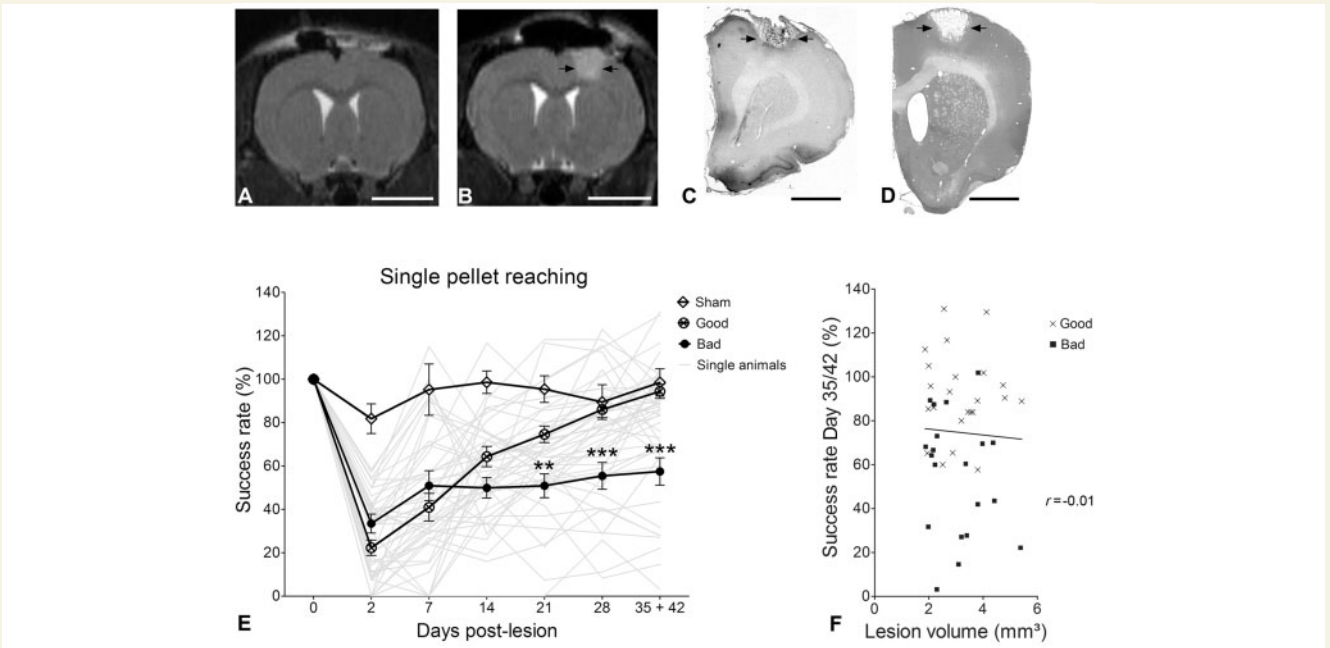

Figure 1 Multiple stereotaxic intracortical injections of endothelin-1 destroy the forelimb motor cortex leading to functional deficits. Cross-sections through the caudal forelimb area with T_2-weighted MRI scans taken 24 h post-lesion show minimal damage in sham-operated animals (**A**) and a hypo-dense region centred on the primary motor cortex in animals receiving a stroke (**B**, black arrows). Cellular damage throughout the layers of the cortex was confirmed with cresyl violet staining of the rostral (**C**, black arrows) and caudal (**D**, black arrows) forelimb area of lesioned animals (49 days post-lesion). (**E**) Endothelin-1-induced stroke lesions lead to a marked deficit on the single pellet grasping task 2 days after the lesion. Animals showed variable recovery courses, with some animals recovering well ('Good': >50% change from Day 2 to Day 35/42 post-lesion, open circles, $n = 23$) and others badly ('Bad': <50% change from Day 2 to Day 35/42 post-lesion, closed circles, $n = 20$). Single animals appear in light grey and group averages in black. (**F**) Despite some variation in lesion size, there was no correlation between the lesion volume and the success rate on the single pellet grasping task at Day 35/42. Animals showing good recovery ($n = 23$) are represented with crosses and those with bad recovery ($n = 20$) with filled squares. Scale bars: **A**, **B** = 5 mm, **C** = 2 mm, **D** = 2.5 mm. Data are presented as means ± SEM; asterisks indicate significances: $^{**}P \leqslant 0.01$, $^{***}P \leqslant 0.001$.

by 3D reconstruction of the lesions in the individual animals (1.86–5.42 mm^3; mean 3.1 ± 0.13 mm^3; $n = 71$, $P > 0.05$, $r = 0.01$, Spearman correlation, Fig. 1F). Additionally, there was no correlation ($P > 0.05$, $r = 0.19$, Spearman correlation) between the pre-lesion and post-lesion success rate when the raw data were used (as opposed to per cent of baseline).

Identification of corticospinal tract neurons projecting to the forepaw area of the spinal cord (C6–C7) in intact rats and following large forelimb strokes

Lesioned animals were retrogradely traced with multiple unilateral injections of Fast blue into the grey matter of cervical spinal cord segments C6–C7 on the denervated side of the spinal cord (Supplementary Fig. 1A–C). Each tracer injection site in every animal was examined in detail and animals where any of the injections either hit the main portion of the CST in the dorsal funiculus or where tracer diffused across the midline to the intact side of the spinal cord were excluded from the study (22 of 75 traced animals excluded).

Two dimensional representations of 3D reconstructions of the Fast blue-labelled layer V forepaw CST cells in trained sham-lesioned animals ($n = 8$) showed the typical pattern of the forelimb innervation (Fig. 2A and C). The majority of the neurons were localized in the caudal ('ipsilesional') forelimb area (4957.9 ± 619.3 Fast blue-labelled cells), rostral forelimb area (1275.8 ± 194.7 Fast blue-labelled cells), S2 (806.6 ± 83.8 Fast blue-labelled cells), contralesional forelimb area (542.3 ± 86.6 Fast blue-labelled cells) and ipsilesional hindlimb field (1719.0 ± 87.5 diamidino yellow dihydrochloride-labelled cells). There were few Fast blue-labelled projecting neurons in the hindlimb field (114.9 ± 37.1 Fast blue-labelled cells).

In the acutely lesioned animals, 2 days survival after the stroke ($n = 4$, Fig. 2B and C), the bulk of the caudal forelimb neurons (1192.5 ± 117.5 Fast blue-labelled cells remaining) and a majority of the rostral forelimb area neurons (434.3 ± 127.1 Fast blue-labelled cells remaining) were destroyed (total 1626.8 ± 172.8 Fast blue-labelled cells remaining). Comparisons with the data from sham animals showed that acutely lesioned animals had significantly fewer Fast blue-labelled cells in the rostral forelimb area ($P < 0.05$, Mann–Whitney test) and in the medial and lateral caudal forelimb area ($P < 0.01$, Mann–Whitney test). However, the most lateral, sensory area S2 was largely spared (Fig. 2B and C, 573.8 ± 26.6 Fast blue-labelled cells remaining), as were the cells in the contralesional cortex (265.5 ± 35.0 Fast blue-labelled cells remaining). As with sham animals, there were very few Fast

Table 1 Grasping success rate (%) and number of Fast blue-labelled cells in different regions of the ipsilesional cortex in chronic lesioned animals

	Animal number	Success rate Day 35/42 (%)	RFA	Medial CFA	Lateral CFA	S2	HL area
bad	412	3.2	54	288	396	963	126
	414	14.6	90	63	702	360	99
	400	22.2	342	18	837	693	36
	126	31.7	504	81	1260	621	135
	416	43.5	630	162	828	513	207
	156	64.3	504	180	477	945	81
	388	66.7	1170	216	1224	639	693
	146	68.2	1233	576	4140	1152	99
recovery	243	86.1	252	126	936	369	297
	403	87.5	558	225	1566	1071	288
	415	88.9	144	180	954	477	333
	411	90.4	333	0	324	1143	144
	244	95.8	189	189	936	558	279
	393	96.2	423	477	1188	1449	306
good	160	105.0	612	99	1179	666	405
	161	112.5	369	333	1611	936	207

The table shows the total number of Fast blue retrogradely labelled cells 49 days after the stroke. Animals are ranked from the worst (*top*) to the best (*bottom*) recovery on the single pellet reaching task at Day 35/42 (columns 1–2). The number of Fast blue-labelled cells in any of the four forelimb regions (columns 3–6) was not correlated with good or bad recovery. However, the number of cells in the hindlimb area (column 7) was.
RFA = rostral forelimb area; CFA = caudal forelimb area; HL area = hindlimb sensorimotor area.

blue-labelled i.e. C6-C7 projecting neurons in the hindlimb field (Fig. 2B and C, 90.0 ± 11.6 Fast blue-labelled cells).

In the chronic lesioned animals ($n = 16$) traced 6 weeks post-lesion, the organization of the C6–C7-projecting cortical neurons was broadly similar to that of the acute animals; for example, in the rostral and caudal forelimb area, the number of retrogradely labelled CST neurons remaining was 462.9 ± 84.8 and 1360.7 ± 248.8, respectively, which was not significantly different from those of the acutely lesioned animals (Fig. 2B–D). As in the acute animals, the lateral S1 and S2 regions were largely spared (784.7 ± 79.3 Fast blue-labelled cells remaining, Fig. 2C and D). Of particular interest was the contralesional cortex where surprisingly we did not detect a significant difference in the number of ipsilaterally projecting neurons (330.8 ± 45.1 Fast blue-labelled cells remaining) between all three groups (intact, acute and chronically lesioned, Fig. 2A–D). An important difference between intact or acute animals and chronic was found in the ipsilesional hindlimb field: in sham and acute animals a mean of 114.9 ± 37.1 ($n = 8$) and 90.0 ± 11.6 ($n = 4$) neurons projected to the cervical spinal cord, respectively, whereas chronically lesioned animals had a significantly higher number of forelimb-projecting cells in the hindlimb field, 285.8 ± 35.2 (Fig. 2C, $n = 16$). This corresponds to an increase of 149% and 218% in comparison to sham and acute animals, respectively. These cells were scattered over all regions of the hindlimb sensory–motor area (Fig. 2D).

Correlation of retrogradely labelled corticospinal tract neuron patterns with behavioural recovery

We correlated the behavioural outcome 5–6 weeks after the stroke with the numbers of retrogradely labelled C6–C7-projecting CST neurons in the different parts of the ipsi- and contralesional cortex for all the individual animals of the chronic lesion group (Fig. 2E–J and Supplementary Fig. 2). Five cortical regions were used for the analysis: the lesioned (ipsilesional) medial and lateral caudal forelimb areas, the rostral forelimb area, S2, the contralesional cortex and the ipsilesional hindlimb sensory–motor area. There was no correlation found between the behavioural recovery and the numbers of cells in the contralesional cortex ($P > 0.05$, $r = 0.24$, Spearmann correlation, Fig. 2E). The same was true for the total number of cells in the ipsilesional cortex ($P > 0.05$, $r = 37$, Spearmann correlation, Fig. 2F) and also the forelimb regions in the ipsilesional cortex ($P > 0.05$, $r = 39$, Spearmann correlation, Fig. 2G). However, strong correlations were seen between the increased numbers of neurons from the ipsilesional hindlimb field projecting to the cervical spinal cord and the success rate ($P < 0.05$, $r = 0.61$, Spearmann correlation, Fig. 2H), as well as the precision of pellet reaching ($P < 0.01$, $r = 0.71$, Spearmann correlation, Fig. 2I).

Anterograde tracing of the hindlimb sensory–motor cortex revealed increased projections to the cervical spinal cord, correlated with high functional recovery

The anterograde axonal tracer biotinylated dextran amine was injected into the ipsilesional hindlimb sensory–motor area in a subset of acutely ($n = 4$) and chronically lesioned animals ($n = 23$), and the cervical spinal cord was analysed to quantify the labelled CST fibres and collateral branches. In naïve animals, the vast majority of the hindlimb sensory–motor cortex CST axons traverse the

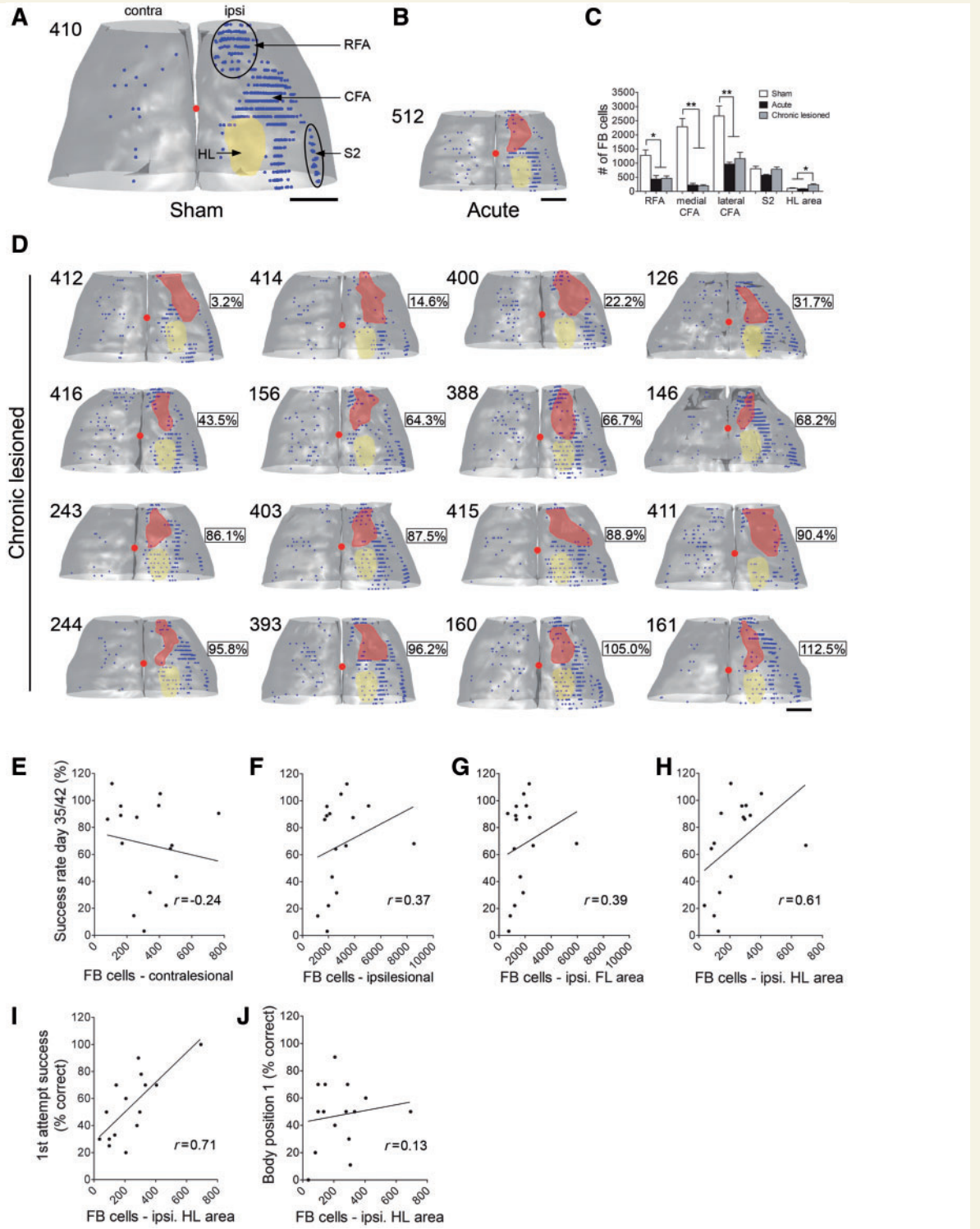

Figure 2 Fast blue (FB) retrograde tracing of cells from the cervical C6–C7 spinal cord. (**A**) Representative 2D representations of the 3D reconstruction of Fast blue-labelled cells in a sham-lesioned animal, viewed from above. Large numbers of Fast blue-labelled cells (blue dots) are found on the ipsilesional (*right*) rostral (RFA) and caudal forelimb area (CFA) and in the secondary somatosensory cortex S2. Few labelled cells are present in the contralesional cortex (*left*) representing the very minor ipsilateral projection of the CST. Also, very few labelled cells are present in the hindlimb sensory–motor cortex (HL; yellow oval). (**B**) Reconstruction of Fast blue-labelled cells in a lesioned animal acutely after the stroke. The lesion (red, shaded area) has largely destroyed the rostral forelimb area (FL) and medial (motor) caudal forelimb area neurons, sparing S2 and the hindlimb field. (**C**) Quantification of the C6–C7-projecting CST neurons in the rostral forelimb area, medial and lateral caudal forelimb area, S2 and hindlimb of intact ($n = 10$), acute ($n = 4$) and chronically lesioned ($n = 16$) rats. (**D**) Maps of C6–C7-projecting CST neurons in 16 chronically lesioned rats arranged from *top left* (Rat 412) to *bottom right* (Rat 161) in rows from the worst success rate on the single pellet reaching test at Day 35/42 (Rat 412, 3.2%) to the best (Rat 161, 112.5%).

(continued)

cervical spinal cord in a straight manner, sending few, if any, collaterals into the grey matter (Fouad *et al.*, 2001). The same situation was found in animals analysed immediately after the stroke (acutely lesioned; Fig. 3A and H). However, in the chronic stroke animals, the number of collaterals leaving the main CST and entering the grey matter in the C2–C7 region of the spinal cord was significantly increased in the majority of, but not all, rats (Fig. 3B–D and H). We correlated the number of cervical spinal cord collaterals of fibres originating in the hindlimb field to the behavioural recovery of each individual animal. A weak, but significant, correlation was found for success rate ($P < 0.05$, $r = 0.50$, Pearson correlation, Fig. 3E) and for correct body position in front of the grasping window ($P < 0.01$, $r = 0.56$, Pearson correlation, Fig. 3F).

Retrograde tracing of the fore- and hindlimb sensory–motor cortex revealed that the majority of reorganized hindlimb cells are connected purely to the cervical spinal cord

We were interested in whether the reorganized hindlimb cells retained their original connection to the lumbar spinal cord or whether this was instead retracted or lost in favour of the new connection to the cervical spinal cord. To investigate this, we carried out a double retrograde tracing of the spinal cord with Fast blue injected into the cervical spinal cord and tetramethylrhodamine injected into the lumbar spinal cord in intact rats and in a group of chronically lesioned animals that showed good recovery. We only reported data from animals that showed good recovery (>60% success rate at Day 35/42), as we had already established in previous experiments (Figs. 2 and 3) that poorly recovering animals (⩽40% success rate at Day 35/42) did not show reorganization of the hindlimb area and so we would not expect to find double-labelled cells.

Double-labelled cells, which had transported the tracers from both the lumbar and cervical spinal cord, were very rare in the intact, normal control rat hindlimb field (13.5 ± 5.8 cells, Fig. 4A–D and G). Their number was increased 6.8-fold 6–8 weeks after the forelimb stroke (85.5 ± 20.9 cells, Fig. 4A–C, E and G), which was significantly more than normal control animals ($P < 0.05$, Mann–Whitney test, Fig. 4G). The double-labelled cells were spread throughout the hindlimb area (Fig. 4E). Interestingly, of the total number of hindlimb field neurons projecting to the cervical spinal cord in the chronic stroke animals (390.4 ± 69.7 cells, Fig. 4F), only 21.9% were double labelled, suggesting that in the majority of cases, reorganized hindlimb cells retracted/lost their original connection to the lumbar spinal cord and instead became solely connected to the cervical spinal cord. In normal control animals, 13.3% of hindlimb neurons projecting to the cervical spinal cord were double labelled (Fig. 4F).

Stimulation of hindlimb sensory–motor cortex elicits forelimb movements in rats with good recovery of function

We mapped the hindlimb and the most caudal region of the caudal forelimb representation with ICMS and recorded fore- as well as hindlimb movements. We carried out ICMS experiments in a subset of lesioned (6 weeks post-lesion; different levels of recovery of skilled pellet reaching) and normal control animals; all animals were randomly number coded and the experimenter was blinded to the code. ICMS maps are shown in Fig. 5A and D. Each circle in the map plots the inverse threshold for evoking a forelimb (blue), hindlimb (yellow) or fore- as well as hindlimb (red) response at each site. The larger the circle the lower the current required to evoke a motor response. Grey dots indicate sites where no movements were evoked at the highest current (90 μA). Despite choosing 90 μA as the maximal current this was rarely the lowest threshold for a movement, particularly at sites where fore- and hindlimb responses were reported. Instead the average maximal movement threshold currents were as follows: forelimb (at a forelimb only site): 52.4 ± 3.8 μA; hindlimb (at a hindlimb only site): 58.9 ± 2.1 μA; forelimb (at a forelimb/hindlimb site): 56.9 ± 4.0 μA; hindlimb (at a forelimb/hindlimb site): 52.9 ± 3.2 μA. Normal control animals ($n = 8$) showed the typical pattern of well separated fore- and hindlimb motor areas (Fig. 5A) with minimal overlap along the border between the two fields and relatively consistent maps between individuals. The average number of sites producing combined forelimb/hindlimb movements in these animals was 4.4 ± 1.0. In the chronic stroke animals ($n = 8$), there was considerable variation between individuals.

Figure 2 Continued

Success rates at Day 35/42 appear in a box on the *right* side of each reconstruction. With increasing success rate, animals show increased numbers of Fast blue-labelled cells in their hindlimb areas (yellow shaded areas). Red shaded areas represent the lesions. (**E–J**) Correlations between behavioural performance in the skilled reaching test and C6–C7-projecting neurons in different cortical areas. There was no significant correlation between the number of Fast blue-labelled cells on the contralesional (*left* in image) cortex of chronic lesioned animals ($n = 16$) and the success rate at Day 35/42 (**E**, $P > 0.05$, $r = 0.24$, Spearmann correlation); neither was there a correlation between the total number of Fast blue-labelled cells on the ipsilesional (*right*) cortex of chronic lesioned animals ($n = 16$) and the success rate at Day 35/42 (**F**, $P > 0.05$, $r = 0.37$, Spearmann correlation) nor was there a correlation between the number of Fast blue-labelled cells in the ipsilesional forelimb area and grasping success (**G**, $P > 0.05$, $r = 0.39$, Spearmann correlation). However, there was a positive correlation ($P < 0.05$, $r = 0.61$, Spearmann correlation) between the number of Fast blue-labelled cells in the ipsilesional hindlimb area (yellow shaded area) of chronic lesioned animals ($n = 16$) and the success rate at Day 35/42 (**H**) and with the first attempt success rate at Day 35/42 ($P < 0.01$, $r = 0.71$, Spearmann correlation) (**I**) but no correlation between the number of Fast blue-labelled cells in the ipsilesional hindlimb area of chronic lesioned animals ($n = 16$) and body position 1 (**J**, $P > 0.05$, $r = 0.13$, Spearmann correlation). Small red circles represent Bregma. Scale bars: **A**, **B** and **D** = 2 mm. Data are presented as means ± SEM; asterisks indicate significances: $*P \leqslant 0.05$, $**P \leqslant 0.01$.

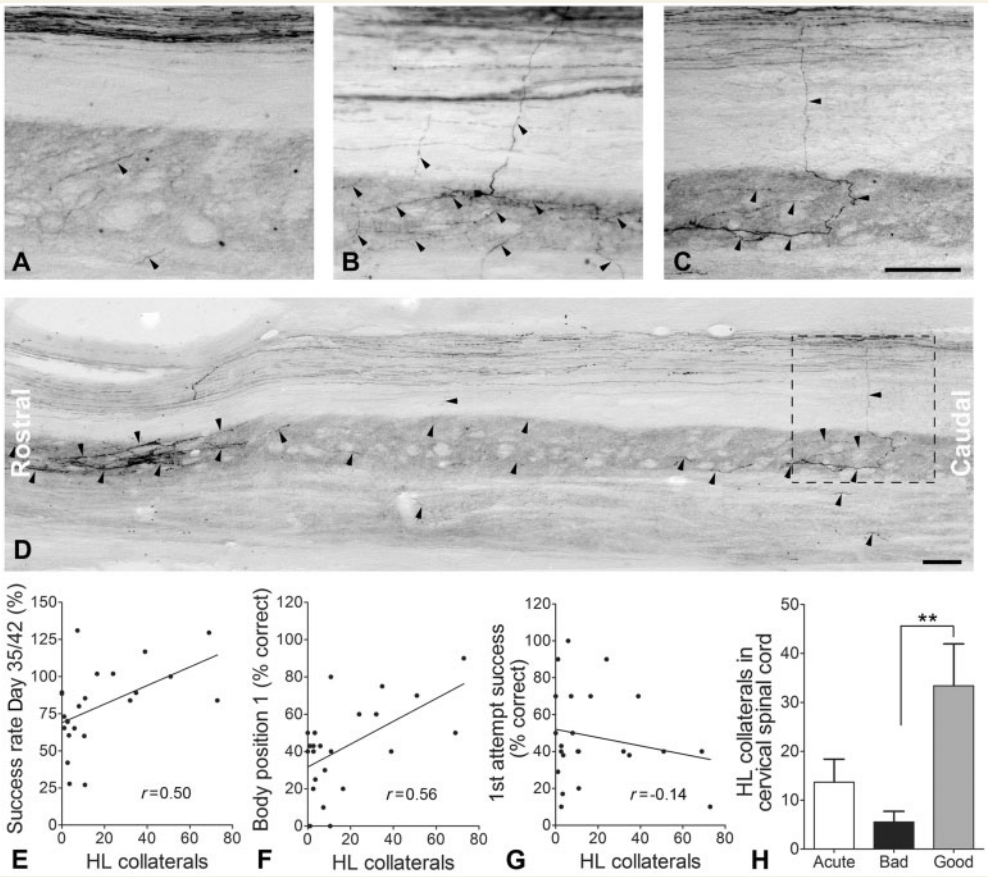

Figure 3 Biotinylated dextran amine anterograde tracing of collaterals from the hindlimb (HL) sensory–motor cortex in the cervical spinal cord. (**A**) Horizontal section shows biotinylated dextran amine-labelled hindlimb fibres travelling through the cervical spinal cord of acutely lesioned ($n = 4$) animals in a compact bundle sending only few collaterals into the grey matter of the cervical spinal cord (black arrowheads). (**B** and **C**) Collaterals from hindlimb-originating fibres can be seen frequently in chronic stroke animals with good recovery of function. Fibres arborize in the grey matter (black arrowheads). (**D**) Low magnification image of the cervical spinal cord of an animal showing good recovery of function (dashed box indicates region of panel **C**). The collaterals of biotinylated dextran amine-labelled hindlimb fibres can be seen throughout the length of the spinal cord (black arrowheads). In horizontal sections of the spinal cord segments C1–T1 'stem' collaterals were counted at the white/grey matter interface and normalized to biotinylated dextran amine-labelled axons in the brainstem. Results are expressed as a collateralization index, i.e. the mean of the total number of stem collaterals in the cervical spinal cord. (**E–G**) There was a positive correlation between the numbers of biotinylated dextran amine-labelled hindlimb collaterals in the cervical spinal cord and the success rate for skilled reaching at Day 35/42 ($P < 0.05$, $r = 0.50$, Spearmann correlation, **E**) as well as with the most perfect body position for grasping ($P < 0.01$, $r = 0.56$, Spearmann correlation, **F**), but not with the first attempt success (**G**, $P > 0.01$, $r = 0.14$, Spearmann correlation). (**H**) Group averages show that animals showing good recovery of function ($n = 12$, grey bar) on the single pellet grasping test at Day 35/42 had significantly more biotinylated dextran amine-labelled hindlimb collaterals in the cervical spinal cord than those animals that recovered badly ($n = 11$, black bar). Scale bars: **A–D** = 200 μm. Data are presented as means ± SEM; asterisks indicate significances: $^{**}P \leqslant 0.01$.

Interestingly, animals showing many forelimb responses elicited in the original hindlimb sensory–motor area were mostly those with good recovery of forelimb function at Day 35/42 (Fig. 5D). The correlation of the number of combined forelimb and hindlimb responses in the hindlimb field with the behavioural outcome is shown in Fig. 5C ($P < 0.01$, $r = 0.85$, Spearman correlation). There was no correlation between baseline success rate on the single pellet grasping task and the post-lesion ICMS maps, i.e. it is not the case that animals that performed best before the lesion recovered better afterwards. These results suggest that many of the hindlimb cells that rewired to the cervical spinal cord as a consequence of the forelimb stroke made functional connections.

Discussion

The outcome following stroke in humans is highly variable, ranging from lifelong hemiplegia to almost complete recovery (Brown and Schultz, 2010; Stinear, 2010; Langhorne *et al.*, 2011), but the reasons for this variation and the exact mechanisms underlying it remain unknown. Both clinical and preclinical data suggest that the size and location of the lesion are key determinants of deficit and recovery potential. Following small (subtotal) lesions to the motor cortex, takeover of functions by other intact areas plays a crucial compensatory role in recovery. Compensatory takeover can occur (i) by remaining spared parts with corresponding functions,

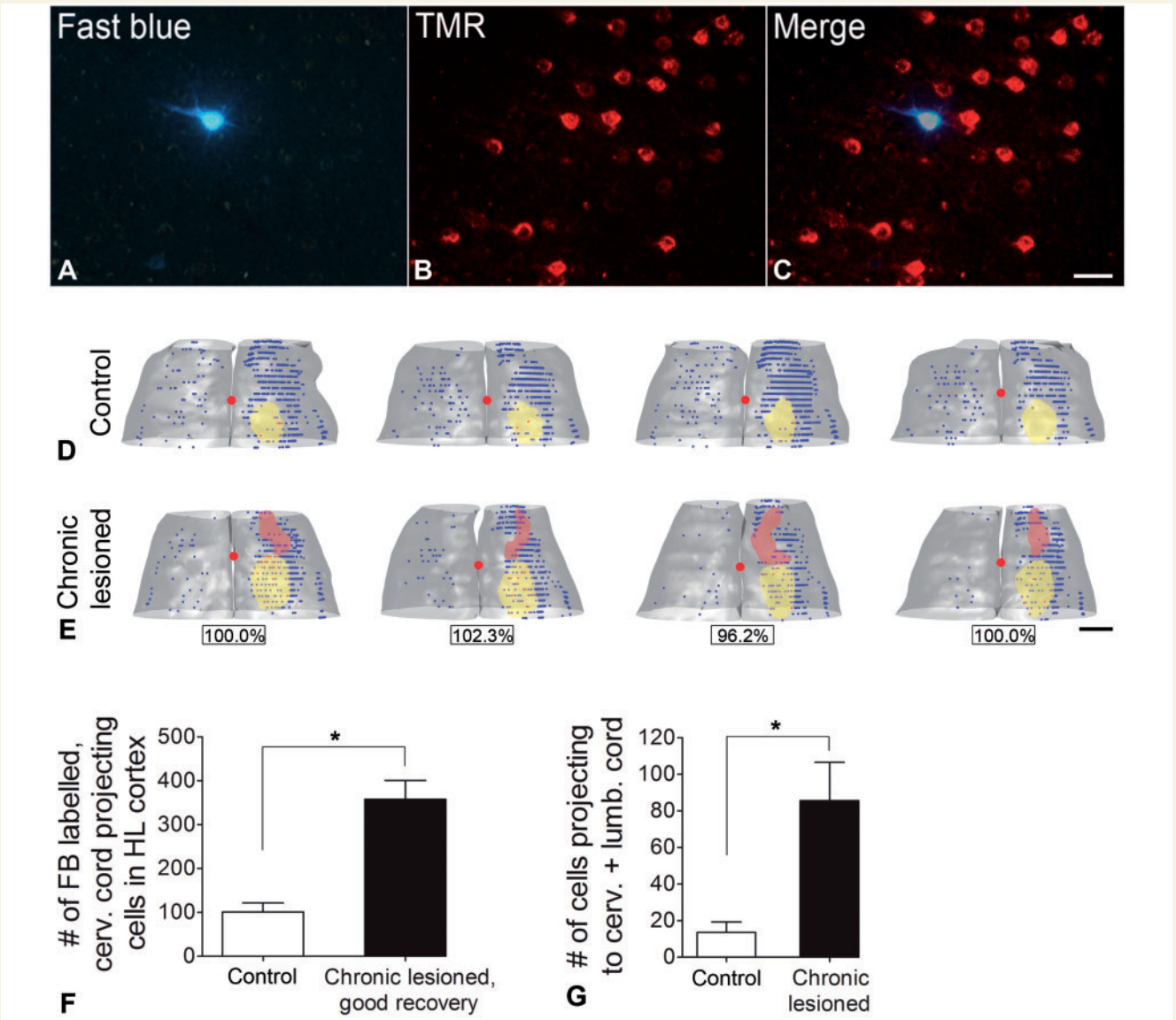

Figure 4 Retrograde double labelling of corticospinal neurons from the cervical (Fast blue, FB) and lumbar (tetramethylrhodamine, TMR) spinal cord. (**A**) A high-power photomicrograph of a Fast blue-labelled pyramidal cell in the hindlimb–sensorimotor cortex. (**B**) Tetramethylrhodamine labelling of the same cell in **A**, and surrounding cells. (**C**) Merge of the Fast blue and tetramethylrhodamine images to show double labelling of the cell. (**D**) 2D representations of the 3D reconstructions of Fast blue-labelled (blue dots) and tetramethylrhodamine-labelled (yellow dots) cells in normal control ($n = 4$) animals. Double-labelled Fast blue and tetramethylrhodamine cells in the hindlimb–sensorimotor cortex appear in red and very few can be seen. (**E**) 2D representations of the 3D reconstructions of Fast blue-labelled (blue dots) and tetramethylrhodamine-labelled (yellow regions) cells in chronic lesioned ($n = 4$) animals showing good recovery of function on the single pellet grasping test at Day 35/42. Success rate appears in a box under each image. Double-labelled Fast blue and tetramethylrhodamine cells in the hindlimb–sensorimotor cortex appear in red. A small number can be seen in each of the animals. (**F**) Quantification of Fast blue labelling in the hindlimb sensorimotor area confirmed that animals showing good recovery of function (black bar) have significantly more Fast blue-labelled cells projecting to the cervical spinal cord than normal control (white bar) animals. (**G**) Quantification of the number of double-labelled cells shows that chronic lesioned, good recovering animals (black bar) have a significantly higher percentage than normal control animals (white bars). Yellow shaded areas on right side of brains indicate the hindlimb sensory–motor area. Small red circles represent Bregma. Scale bars: **A–C** = 150 μm, **D** and **E** = 2 mm. Data are presented as means ± SEM; asterisks indicate significances: $*P \leqslant 0.05$.

e.g. the face motor cortex compensating for the hand motor cortex (Donoghue and Sanes, 1988; Castro-Alamancos *et al.*, 1992; Castro-Alamancos and Borrel, 1995; Wu and Kaas, 1999); or (ii) by contralateral intact cortical areas with the same function (Barth *et al.*, 1990; Xerri *et al.*, 1998; Whishaw, 2000; Feydy *et al.*, 2002; Werhahn *et al.*, 2003).

Using multiple injections of the vasoconstrictor endothelin-1, we destroyed >70% of the caudal and rostral motor forelimb area of

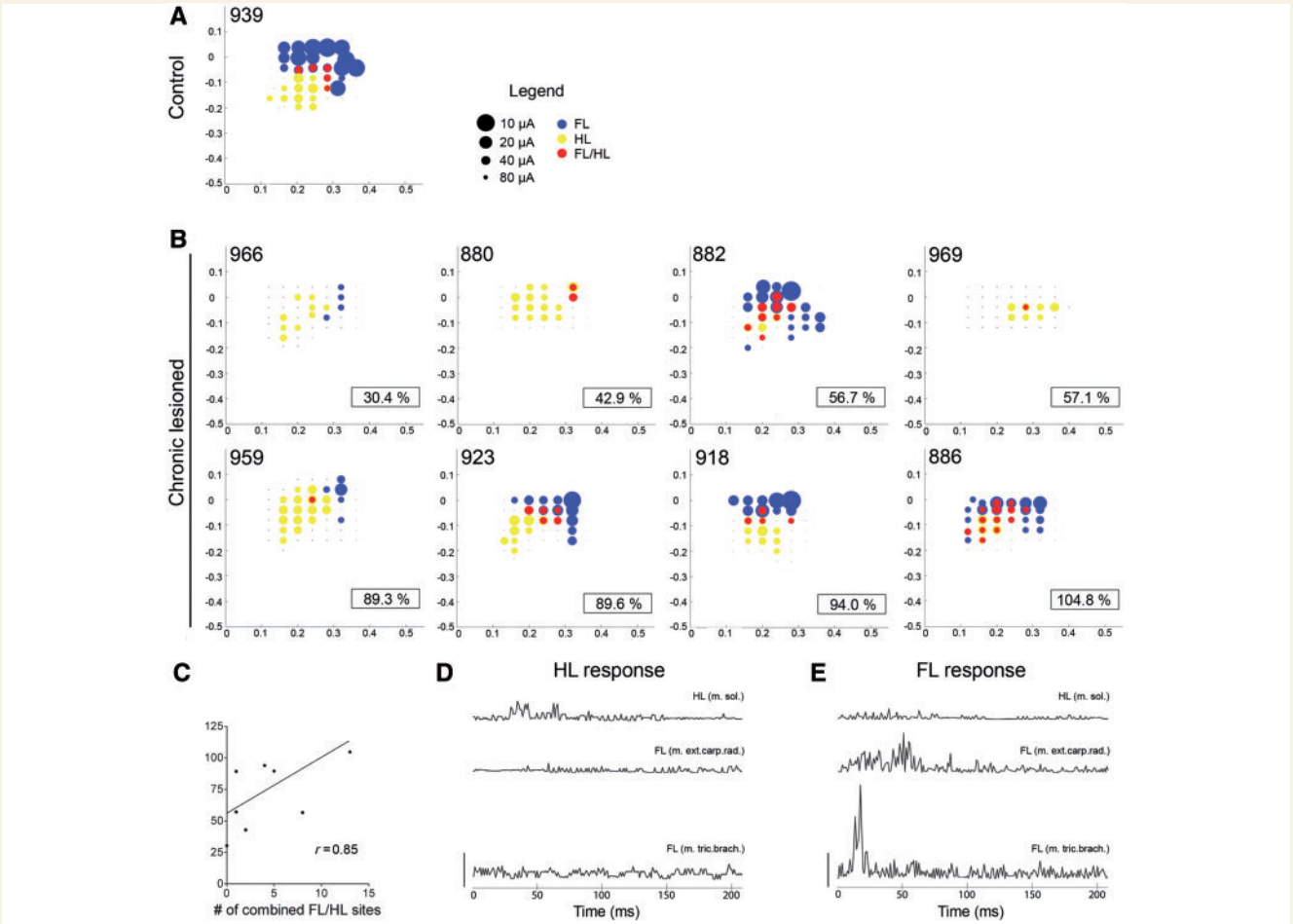

Figure 5 ICMS maps of the hindlimb sensorimotor area of normal control ($n = 8$) (**A**) and chronically lesioned ($n = 8$) (**C**) animals. *x*-axis: distance lateral to Bregma; *y*-axis: distance caudal of Bregma; forelimb response (blue circles), hindlimb response (yellow circles) and both fore-/hindlimb response (red circles); circle size is inversely related to the threshold for evoked forelimb response; circle opacity represents percentage of electrode penetrations evoking a response at that site; grey dots are sites where no response was evoked using currents up to 90 µA. All electrode penetration sites are separated from adjacent penetrations by 400 µm distance in rostrocaudal and mediolateral directions. For chronic lesioned animals (**C**), the success rate on the single pellet grasping task at Day 35/42 appears in the bottom right corner of the ICMS map. (**A**) Average bubble plot of all normal control animals ($n = 8$). (**B**) ICMS maps of all chronic lesioned animals ($n = 8$). Bubble plots are arranged from left to right in rows from the worst success rate on the single pellet reaching test at Day 35/42 (Rat 966, 30.4% success rate) to the best (Rat 886, 104.8% success rate). With increasing success rate, animals show increased numbers of forelimb responses (red circles) at sites that also elicited hindlimb responses (yellow circles). (**C**) There was a strong positive correlation in the chronic stroke group between the number of combined forelimb/hindlimb responses and the success rate on the single pellet reaching test at Day 35/42 ($P < 0.01$, $r = 0.85$, Spearman correlation). (**D**) Example EMG data showing a hindlimb response: a response can be seen in the hindlimb (m. sol) with no responses in the forelimb (m. ext. carp.rad. and m. tric.brach.). (**E**) Example EMG data showing a forelimb response, no response can be seen in the hindlimb (m. sol) whereas a clear response is seen in the forelimb (m. ext. carp.rad. and m. tric.brach.). Calibration bars: **D** and **E** = 0.1 mV. FL = forelimb response; HL = hindlimb response, FL/HL = combined forelimb and hindlimb response.

adult rats. Skilled forepaw reaching behaviour recovered, with large variations among animals, over 2–6 weeks post-stroke. Injections of a highly efficient retrograde tracer into the spinal cord identified new and spared forelimb-connected corticospinal neurons. Surprisingly, a significant number of neurons in the hindlimb sensory–motor cortex established connections to the cervical spinal cord as a consequence of the lesion; in individual animals their number was correlated with the degree of recovery of forelimb function. Intracortical microstimulations suggested that the new connections from the hindlimb were functional, and double retrograde tracing suggested that the original connection of these cells to the lumbar spinal cord was lost. These results show that map shifts in the motor cortex can be as drastic (from hindlimb to forelimb) and can involve sprouting, branch formation and new circuits of cortical output axons in the spinal cord.

In the present study, the lesions largely, but not completely, destroyed the main (caudal) as well as the premotor (rostral) forelimb cortex by the endothelin-1-induced ischaemia. The behavioural outcome for skilled forelimb reaching at 6 weeks after the stroke was highly variable, from very good to greatly impaired.

The lesion left a variable number of CST neurons with an intact connection to the cervical spinal cord as shown by retrograde tracing. Interestingly, no correlation was found between the numbers of these spared CST neurons in the caudal or rostral forelimb areas and the behavioural recovery of the individual animals. The same was true for the small number of ipsilaterally projecting CST neurons in the contralesional hemisphere; the number of these neurons did not change as a consequence of the lesion, and there was no correlation between their number and behavioural recovery. However, a very different situation occurred in the ipsilesional spared hindlimb sensory–motor cortex where few cells project to the cervical spinal cord/forelimb in intact rats. On average this number was more than doubled in the chronic stroke rats, and there was a strong correlation between the number of hindlimb CST neurons projecting to the cervical spinal cord and the functional recovery of individual animals.

Increased numbers of Fast blue-labelled cells in the hindlimb sensory–motor area might also have resulted from terminal sprouting of fibres from forelimb-projecting cells in the hindlimb sensory–motor area, which had only a small axonal arbour not sufficient for dye uptake prior to the lesion. However, this explanation is unlikely because stem collaterals were rare in naive animals, in our controls and in those animals that recovered badly. Therefore, even if arborization in the grey matter would have been insufficient to pick up detectable amounts of Fast blue, the stem collateral giving rise to the sprouting would still have been detected by the anterograde tracing. Additionally, we had a high number of animals in each group, we did not see many Fast blue-labelled cells in the hindlimb sensory–motor area in the control/acute groups and we report strong correlations between grasping success and the number of these cells. Thus, this threshold of sprouting explanation seems unlikely.

It is known that cortical motor areas exhibit considerable interindividual spatial variability (Kline and Reid, 1984) and that they are influenced by behavioural experience and training (Kleim *et al.*, 1998, 2004; Adkins *et al.*, 2006; Wang *et al.*, 2011), which could have influenced our lesion coordinates. However, these two concerns were dealt with by using high animal numbers for each part of the study and by all animals that were used being trained on the single pellet reaching task. This led to low interindividual variability, e.g. cell counts were similar, and ICMS map locations were similar. Consideration was also given to other cortical mapping techniques, but all available techniques had negative aspects, e.g. with functional MRI only the location of the sensory cortex is known, and the technique has a low spatial resolution, voltage-sensitive dye imaging is a terminal procedure, ICMS mapping before the lesion may have caused small amounts of damage to the cortex and intrinsic optical imaging also gives only the sensory cortex. This is an issue because although there is an almost complete overlap of hindlimb sensory responses with the hindlimb motor cortex, this is not the case for the forelimb cortex where the medial aspects are purely motor and it is only in the lateral aspects that there is overlap with the forelimb sensory areas (Donoghue and Wise, 1982). Thus, accurately locating the area of the forelimb sensory region does not accurately locate the forelimb motor region. As it was not possible to use the ICMS mapping technique on an individual basis, owing to potential damage to the cortex by electrode penetrations, we chose tracing because this was the method we used for analysis.

Anterograde tracing confirmed previous results (Fouad *et al.*, 2001) that collaterals branching off the hindlimb-projecting CST in the cervical spinal cord are normally rare in intact animals. In contrast, a much higher number of collaterals establishing highly branched terminal networks in the cervical grey matter were observed in chronic stroke rats. Again, there was a high variation among individuals but a significant correlation between the number of stem collaterals, which gave rise to branched terminals, and forelimb performance. These anatomical observations therefore suggest that a significant contributor to functional recovery of skilled reaching after selective forelimb strokes comes from the hindlimb sensory–motor cortex. Although these cells are small in number, they branch extensively in the cervical grey matter and their contribution to functional recovery seems more important than the role of remaining, possibly functionally impaired, caudal and rostral forelimb area neurons or the intact ipsilateral (contralesional) cortex.

In accordance with many studies in animals and humans, the contralesional cortex plays a minor role in cases of smaller partial strokes (Xerri *et al.*, 1998; Marshall *et al.*, 2000; Whishaw, 2000; Dijkhuizen *et al.*, 2001, 2003; Feydy *et al.*, 2002; Werhahn *et al.*, 2003; Mostany and Portera-Cailliau, 2011). It appears that the overall size of the lesion, and thus the degree of cellular damage, is the reason for this, as following small cortical lesions in rats (Barth *et al.*, 1990) and primates (Xerri *et al.*, 1998), reorganization was seen within the lesioned cortex with no change in the undamaged contralesional cortex. Thus, it is likely that in our case, where the lesions were subtotal for the motor cortex, the intact contralesional cortex played a minor role in recovery, as evidenced by no change in Fast blue-labelled cells on this side of the cortex, compared with the ipsilesional cortex, where a rise in the number of Fast blue-labelled cells in the hindlimb sensory–motor area was observed. Additionally, reorganization to more distant regions ipsilaterally, for example the rostral forelimb area, could also have occurred as has been shown previously (Dancause *et al.*, 2005), but in our case, this is unlikely, as in the majority of the rats the lesions destroyed a large proportion of this region.

ICMS was used to investigate the functionality of the new connections from the hindlimb to the cervical spinal cord. The typical sharp distinction between forelimb and hindlimb motor cortex was found in the intact animals. In the chronic stroke animals, however, forelimb responses were frequently elicited at low current amplitude from the hindlimb field. Again, a correlation existed between these electrophysiological results and behavioural recovery in individual animals. Forelimb as well as hindlimb responses were often obtained from the same stimulation site (albeit at a different depth and/or current), probably due to the fact that a number of CST neurons were excited simultaneously. A maximal current of 90 μA was chosen based on previous publications (Neafsey and Sievert, 1982; Gharbawie *et al.*, 2005; Brus-Ramer *et al.*, 2007); however, this was rarely the lowest movement threshold. Previous studies estimate that a 90 μA stimulus could spread radially from the electrode tip to 300 μm (Asanuma, 1967), thus potentially co-activating both forelimb and hindlimb simultaneously. However, as our stimulation sites were 400 μm apart,

forelimb and hindlimb responses were often at different depths and currents at the particular mapping point and because 90 μA was well above the average current threshold for movement, we think this is not a significant concern for our data. In addition, our results are also in line with previous studies, e.g. it was shown that following a stroke to the forelimb area, forelimb movements could be evoked from the original hindlimb area in well recovered animals (Castro-Alamancos and Borrel, 1995). Using *in vivo* calcium imaging following selective strokes, it was shown that individual somatosensory neurons altered their input selectivity, either from fore- to hindlimb or from a single to multiple limbs (Winship and Murphy, 2008). In primates and rats following deafferentation by arm amputation, the forelimb area of M1 became fully filled in with adjacent body representations (Donoghue and Sanes, 1988; Wu and Kaas, 1999). Similar results are also observed in humans following limb immobilization (Langer *et al.*, 2012), bimanual upper limb training (Hoffman and Field-Fote, 2007) and spinal cord injury (Green *et al.*, 1999).

Double retrograde tracing from the cervical and lumbar spinal cord was used to determine whether hindlimb neurons innervating the cervical spinal cord also connected to the lumbar cord. Interestingly, there were very few double-labelled cells, the majority of neurons in this region, many of which appeared as a consequence of the stroke, were labelled exclusively from the cervical cord. Although it is not possible to make conclusions about presumably activity-dependent axon growth dynamics without an extensive time course study, these results suggest that the original axon to the hindlimb cord was retracted or degraded. Indeed, degeneration of axons has been seen by electron microscopy in the lumbar spinal cord in the similar paradigm (Weishaupt *et al.*, 2010), but further investigation would be required to confirm this for the present results.

As the rat was used as the experimental model in this study the question arises of whether topographical mapping in this species is sufficiently precise to be generally applicable. We believe that it is for several reasons. Firstly, retrogradely labelled cell counts were highly consistent between separate animals, suggesting that sensorimotor cortex anatomy is relatively stable between individual rats. Secondly, the border region between the forelimb and hindlimb sensorimotor cortex was not particularly significant for reorganization, as our results show that reorganized cells were seen throughout the hindlimb area, and their number was highly correlated with grasping success. Thirdly, ICMS experiments were performed in the hindlimb area and there were few forelimb responses in this region in sham/control animals or those that recovered badly. Although it is known that connections through the corpus callosum are present in humans and that they play an important role in inhibition and excitation, this is not known for rodents. We believe, however, that such connections did not play a large role in our experiments because following anterograde tracing we counted the number of 'stem collaterals' (the fibres crossing the white–grey matter boundary) originating from hindlimb cortex fibres and entering the cervical spinal cord. Their increased number in animals with good recovery was not due to branching of arbours in the grey matter but rather due to increases in the number of fibres crossing the white–grey matter boundary.

If forelimb-projecting neurons in the hindlimb sensory motor field are to become fully functional, they have to receive sensory input from the forelimb. Extension of the forelimb sensory map into the hindlimb sensory–motor field after stroke has been described using voltage-sensitive dyes in mouse models (Xerri *et al.*, 1998; Dijkhuizen *et al.*, 2001; Winship and Murphy, 2008; Brown *et al.*, 2009), and recently increased responses in the sensorimotor cortex post-stroke have been linked to motor recovery in humans (Schaechter *et al.*, 2011). Whether pre-existing connections or growth of new horizontal connections are responsible for these map shifts (Li and Carmichael, 2006), and how the specificity of these connections is established, is currently unknown. In a model of thoracic spinal cord injury, a similar map shift of hindlimb to forelimb functions and anatomy has been described. Specifically, hindlimb neurons connected to the cervical spinal cord after transection of their axons in the thoracic cord, and sensory stimulation of the forepaw elicited rapid activation of the hindlimb (as well as forelimb) sensory–motor field (Ghosh *et al.*, 2010).

The molecular mechanisms underlying these impressive anatomical changes are currently unknown. Perilesional regions of the cortex are known to express elevated levels of neurotrophic factors as well as growth-related messenger RNAs and proteins (Stroemer *et al.*, 1993; Keyvani *et al.*, 2002; Lu *et al.*, 2003; Zhao *et al.*, 2006; Li *et al.*, 2010). Additionally, sprouting over significant distances horizontally has been shown (Adesnik and Scanziani, 2010; Brown *et al.*, 2010; Li *et al.*, 2010). Thus, an elevated level of plasticity and growth is probably present in the hindlimb cortex adjacent to the stroke lesions in our model. In the spinal cord, selective lesions of the CST were shown to lead to changes of messenger RNA expression to include growth-related genes (Bareyre and Schwab, 2003; Maier *et al.*, 2008). Finally, activity was shown to regulate CST growth and branching in developing as well as adult injured rats (Martin *et al.*, 1999, 2004; Brus-Ramer *et al.*, 2007; Maier *et al.*, 2008; Carmel *et al.*, 2010). Denervation or the change in functional status of spinal cord neurons after the stroke could induce factors that increase local plasticity and induce/attract sprouting fibres from neighbouring pathways including the hindlimb CST. All these mechanisms, which will require future detailed investigation, probably contribute and collaborate to produce the anatomical and functional changes that lead to behavioural recovery shown in the present experimental paradigm and potentially also the functional recovery observed clinically.

In conclusion, the present results show that large map shifts, e.g. between hindlimb and forelimb, can occur as a consequence of ischaemic destruction of large parts of the sensory–motor cortex in adult rats. Major anatomical changes including rewiring of hindlimb neurons to the forelimb spinal cord occur and probably contribute to functional recovery. These results add to our understanding of structural and functional plasticity after lesions in the adult CNS.

Acknowledgements

The authors thank Marc Bolliger for his help with and loan of the EMG set-up, Eric Rouiller for his expertise in establishing ICMS,

Wendy Kartje and Arko Ghosh for helpful advice and discussion and Mirjam Gullo, Hansjörg Kasper and Stefan Giger for technical support.

Funding

Swiss National Science Foundation (Grant number 3100AO-122527/1); the National Centre for Competence in Research 'Neural Plasticity and Repair' of the Swiss National Science Foundation; The European Union's Seventh Framework Programme FP7/2007-2013 (Grant numbers 201024 and 202213) (European Stroke Network, www.europeanstrokenetwork.info/); The European Commission under the 7th Framework Programme—HEALTH—Collaborative Project Plasticise (www.plasticise.eu) (Grant number 223524) and The Spinal Cord Consortium of the Christopher and Dana Reeve Foundation.

Supplementary material

Supplementary material is available at *Brain* online.

References

Adesnik H, Scanziani M. Lateral competition for cortical space by layer-specific horizontal circuits. Nature 2010; 464: 1155–60.

Adkins DL, Boychuk J, Remple MS, Kleim JA. Motor training induces experience-specific patterns of plasticity across motor cortex and spinal cord. J Appl Physiol 2006; 101: 1776–82.

Adkins DL, Voorhies AC, Jones TA. Behavioral and neuroplastic effects of focal endothelin-1 induced sensorimotor cortex lesions. Neuroscience 2004; 128: 473–86.

Asanuma H, Sakata H. Functional organization of a cortical efferent system examined with focal depth stimulation in cats. J Neurophysiol 1967; 30: 35–54.

Bareyre FM, Schwab ME. Inflammation, degeneration and regeneration in the injured spinal cord: insights from DNA microarrays. Trends Neurosci 2003; 26: 555–63.

Barth TM, Jones TA, Schallert T. Functional subdivisions of the rat somatic sensorimotor cortex. Behav Brain Res 1990; 39: 73–95.

Brown AW, Schultz BA. Recovery and rehabilitation after stroke. Semin Neurol 2010; 30: 511–17.

Brown CE, Aminoltejari K, Erb H, Winship IR, Murphy TH. In vivo voltage-sensitive dye imaging in adult mice reveals that somatosensory maps lost to stroke are replaced over weeks by new structural and functional circuits with prolonged modes of activation within both the peri-infarct zone and distant sites. J Neurosci 2009; 29: 1719–34.

Brown CE, Boyd JD, Murphy TH. Longitudinal in vivo imaging reveals balanced and branch-specific remodeling of mature cortical pyramidal dendritic arbors after stroke. J Cereb Blood Flow Metab 2010; 30: 783–91.

Brown CE, Li P, Boyd JD, Delaney KR, Murphy TH. Extensive turnover of dendritic spines and vascular remodeling in cortical tissues recovering from stroke. J Neurosci 2007; 27: 4101–9.

Brus-Ramer M, Carmel JB, Chakrabarty S, Martin JH. Electrical stimulation of spared corticospinal axons augments connections with ipsilateral spinal motor circuits after injury. J Neurosci 2007; 27: 13793–801.

Carmel JB, Berrol LJ, Brus-Ramer M, Martin JH. Chronic electrical stimulation of the intact corticospinal system after unilateral injury restores skilled locomotor control and promotes spinal axon outgrowth. J Neurosci 2010; 30: 10918–26.

Castro-Alamancos MA, Borrel J. Functional recovery of forelimb response capacity after forelimb primary motor cortex damage in the rat is due to the reorganization of adjacent areas of cortex. Neuroscience 1995; 68: 793–805.

Castro-Alamancos MA, Garcia-Segura LM, Borrell J. Transfer of function to a specific area of the cortex after induced recovery from brain damage. Eur J Neurosci 1992; 4: 853–63.

Cicinelli P, Traversa R, Bassi A, Scivoletto G, Rossini PM. Interhemispheric differences of hand muscle representation in human motor cortex. Muscle Nerve 1997; 20: 535–42.

Dancause N, Barbay S, Frost SB, Plautz EJ, Chen D, Zoubina EV, et al. Extensive cortical rewiring after brain injury. J Neurosci 2005; 25: 10167–79.

Dancause N, Nudo RJ. Shaping plasticity to enhance recovery after injury. Prog Brain Res 2011; 192: 273–95.

Dijkhuizen RM, Ren J, Mandeville JB, Wu O, Ozdag FM, Moskowitz MA, et al. Functional magnetic resonance imaging of reorganization in rat brain after stroke. Proc Natl Acad Sci USA 2001; 98: 12766–71.

Dijkhuizen RM, Singhal AB, Mandeville JB, Wu O, Halpern EF, Finklestein SP, et al. Correlation between brain reorganization, ischemic damage, and neurologic status after transient focal cerebral ischemia in rats: a functional magnetic resonance imaging study. J Neurosci 2003; 23: 510–17.

Donoghue JP, Sanes JN. Organization of adult motor cortex representation patterns following neonatal forelimb nerve injury in rats. J Neurosci 1988; 8: 3221–32.

Donoghue JP, Wise SP. The motor cortex of the rat: cytoarchitecture and microstimulation mapping. J Comp Neurol 1982; 212: 76–88.

Emerick AJ, Neafsey EJ, Schwab ME, Kartje GL. Functional reorganization of the motor cortex in adult rats after cortical lesion and treatment with monoclonal antibody IN-1. J Neurosci 2003; 23: 4826–30.

Enright LE, Zhang S, Murphy TH. Fine mapping of the spatial relationship between acute ischemia and dendritic structure indicates selective vulnerability of layer V neuron dendritic tufts within single neurons in vivo. J Cereb Blood Flow Metab 2007; 27: 1185–200.

Feydy A, Carlier R, Roby-Brami A, Bussel B, Cazalis F, Pierot L, et al. Longitudinal study of motor recovery after stroke: recruitment and focusing of brain activation. Stroke 2002; 33: 1610–17.

Fouad K, Pedersen V, Schwab ME, Brosamle C. Cervical sprouting of corticospinal fibers after thoracic spinal cord injury accompanies shifts in evoked motor responses. Curr Biol 2001; 11: 1766–70.

Gharbawie OA, Gonzalez CL, Williams PT, Kleim JA, Whishaw IQ. Middle cerebral artery (MCA) stroke produces dysfunction in adjacent motor cortex as detected by intracortical microstimulation in rats. Neuroscience 2005; 130: 601–10.

Ghosh A, Haiss F, Sydekum E, Schneider R, Gullo M, Wyss MT, et al. Rewiring of hindlimb corticospinal neurons after spinal cord injury. Nat Neurosci 2010; 13: 97–104.

Gilmour G, Iversen SD, O'Neill MF, Bannerman DM. The effects of intracortical endothelin-1 injections on skilled forelimb use: implications for modelling recovery of function after stroke. Behav Brain Res 2004; 150: 171–83.

Green JB, Sora E, Bialy Y, Ricamato A, Thatcher RW. Cortical motor reorganization after paraplegia: an EEG study. Neurology 1999; 53: 736–43.

Hennig J, Nauerth A, Friedburg H. RARE imaging: a fast imaging method for clinical MR. Magn Reson Med 1986; 3: 823–33.

Herzog A, Brosamle C. 'Semifree-floating' treatment: a simple and fast method to process consecutive sections for immunohistochemistry and neuronal tracing. J Neurosci Methods 1997; 72: 57–63.

Hewlett KA, Corbett D. Delayed minocycline treatment reduces long-term functional deficits and histological injury in a rodent model of focal ischemia. Neuroscience 2006; 141: 27–33.

Hoffman LR, Field-Fote EC. Cortical reorganization following bimanual training and somatosensory stimulation in cervical spinal cord injury: a case report. Phys Ther 2007; 87: 208–23.

Kaas JH, Qi HX, Burish MJ, Gharbawie OA, Onifer SM, Massey JM. Cortical and subcortical plasticity in the brains of humans, primates, and rats after damage to sensory afferents in the dorsal columns of the spinal cord. Exp Neurol 2008; 209: 407–16.

Keyvani K, Witte OW, Paulus W. Gene expression profiling in perilesional and contralateral areas after ischemia in rat brain. J Cereb Blood Flow Metab 2002; 22: 153–60.

Kleim JA, Barbay S, Nudo RJ. Functional reorganization of the rat motor cortex following motor skill learning. J Neurophysiol 1998; 80: 3321–5.

Kleim JA, Hogg TM, VandenBerg PM, Cooper NR, Bruneau R, Remple M. Cortical synaptogenesis and motor map reorganization occur during late, but not early, phase of motor skill learning. J Neurosci 2004; 24: 628–33.

Kline J, Reid KH. Variability of bregma in 300 g Long-Evans and Sprague-Dawley rats. Physiol Behav 1984; 33: 301–3.

Langer N, Hanggi J, Muller NA, Simmen HP, Jancke L. Effects of limb immobilization on brain plasticity. Neurology 2012; 78: 182–8.

Langhorne P, Bernhardt J, Kwakkel G. Stroke rehabilitation. Lancet 2011; 377: 1693–702.

Li S, Carmichael ST. Growth-associated gene and protein expression in the region of axonal sprouting in the aged brain after stroke. Neurobiol Dis 2006; 23: 362–73.

Li S, Overman JJ, Katsman D, Kozlov SV, Donnelly CJ, Twiss JL, et al. An age-related sprouting transcriptome provides molecular control of axonal sprouting after stroke. Nat Neurosci 2010; 13: 1496–504.

Liepert J, Graef S, Uhde I, Leidner O, Weiller C. Training-induced changes of motor cortex representations in stroke patients. Acta Neurol Scand 2000; 101: 321–6.

Liepert J, Miltner WH, Bauder H, Sommer M, Dettmers C, Taub E, et al. Motor cortex plasticity during constraint-induced movement therapy in stroke patients. Neurosci Lett 1998; 250: 5–8.

Lu A, Tang Y, Ran R, Clark JF, Aronow BJ, Sharp FR. Genomics of the periinfarction cortex after focal cerebral ischemia. J Cereb Blood Flow Metab 2003; 23: 786–810.

Maier IC, Baumann K, Thallmair M, Weinmann O, Scholl J, Schwab ME. Constraint-induced movement therapy in the adult rat after unilateral corticospinal tract injury. J Neurosci 2008; 28: 9386–403.

Markus TM, Tsai SY, Bollnow MR, Farrer RG, O'Brien TE, Kindler-Baumann DR, et al. Recovery and brain reorganization after stroke in adult and aged rats. Ann Neurol 2005; 58: 950–3.

Marshall RS, Perera GM, Lazar RM, Krakauer JW, Constantine RC, DeLaPaz RL. Evolution of cortical activation during recovery from corticospinal tract infarction. Stroke 2000; 31: 656–61.

Martin JH, Choy M, Pullman S, Meng Z. Corticospinal system development depends on motor experience. J Neurosci 2004; 24: 2122–32.

Martin JH, Kably B, Hacking A. Activity-dependent development of cortical axon terminations in the spinal cord and brain stem. Exp Brain Res 1999; 125: 184–99.

Mostany R, Portera-Cailliau C. Absence of large-scale dendritic plasticity of layer 5 pyramidal neurons in peri-infarct cortex. J Neurosci 2011; 31: 1734–8.

Murphy TH, Corbett D. Plasticity during stroke recovery: from synapse to behaviour. Nat Rev Neurosci 2009; 10: 861–72.

Neafsey EJ, Bold EL, Haas G, Hurley-Gius KM, Quirk G, Sievert CF, et al. The organization of the rat motor cortex: a microstimulation mapping study. Brain Res 1986; 396: 77–96.

Neafsey EJ, Sievert C. A second forelimb motor area exists in rat frontal cortex. Brain Res 1982; 232: 151–6.

Schaechter JD, van Oers CA, Groisser BN, Salles SS, Vangel MG, Moore CI, et al. Increase in sensorimotor cortex response to somatosensory stimulation over subacute poststroke period correlates with motor recovery in hemiparetic patients. Neurorehabil Neural Repair 2012; 26: 325–34.

Starkey ML, Bleul C, Maier IC, Schwab ME. Rehabilitative training following unilateral pyramidotomy in adult rats improves forelimb function in a non-task specific way. Exp Neurol 2011; 232: 81–9.

Stinear C. Prediction of recovery of motor function after stroke. Lancet Neurol 2010; 9: 1228–32.

Stroemer RP, Kent TA, Hulsebosch CE. Acute increase in expression of growth associated protein GAP-43 following cortical ischemia in rat. Neurosci Lett 1993; 162: 51–4.

Traversa R, Cicinelli P, Bassi A, Rossini PM, Bernardi G. Mapping of motor cortical reorganization after stroke. A brain stimulation study with focal magnetic pulses. Stroke 1997; 28: 110–17.

Wang L, Conner JM, Rickert J, Tuszynski MH. Structural plasticity within highly specific neuronal populations identifies a unique parcellation of motor learning in the adult brain. Proc Natl Acad Sci USA 2011; 108: 2545–50.

Ward NS, Newton JM, Swayne OB, Lee L, Frackowiak RS, Thompson AJ, et al. The relationship between brain activity and peak grip force is modulated by corticospinal system integrity after subcortical stroke. Eur J Neurosci 2007; 25: 1865–73.

Ward NS, Newton JM, Swayne OB, Lee L, Thompson AJ, Greenwood RJ, et al. Motor system activation after subcortical stroke depends on corticospinal system integrity. Brain 2006; 129: 809–19.

Weishaupt N, Silasi G, Colbourne F, Fouad K. Secondary damage in the spinal cord after motor cortex injury in rats. J Neurotrauma 2010; 27: 1387–97.

Werhahn KJ, Conforto AB, Kadom N, Hallett M, Cohen LG. Contribution of the ipsilateral motor cortex to recovery after chronic stroke. Ann Neurol 2003; 54: 464–72.

Whishaw IQ. Loss of the innate cortical engram for action patterns used in skilled reaching and the development of behavioral compensation following motor cortex lesions in the rat. Neuropharmacology 2000; 39: 788–805.

Whishaw IQ, Pellis SM. The structure of skilled forelimb reaching in the rat: a proximally driven movement with a single distal rotatory component. Behav Brain Res 1990; 41: 49–59.

Whishaw IQ, Pellis SM, Gorny B, Kolb B, Tetzlaff W. Proximal and distal impairments in rat forelimb use in reaching follow unilateral pyramidal tract lesions. Behav Brain Res 1993; 56: 59–76.

Winship IR, Murphy TH. In vivo calcium imaging reveals functional rewiring of single somatosensory neurons after stroke. J Neurosci 2008; 28: 6592–606.

Wu CW, Kaas JH. Reorganization in primary motor cortex of primates with long-standing therapeutic amputations. J Neuroscience 1999; 19: 7679–97.

Xerri C, Merzenich MM, Peterson BE, Jenkins W. Plasticity of primary somatosensory cortex paralleling sensorimotor skill recovery from stroke in adult monkeys. J Neurophysiol 1998; 79: 2119–48.

Z'Graggen WJ, Fouad K, Raineteau O, Metz GA, Schwab ME, Kartje GL. Compensatory sprouting and impulse rerouting after unilateral pyramidal tract lesion in neonatal rats. J Neurosci 2000; 20: 6561–9.

Zhang S, Boyd J, Delaney K, Murphy TH. Rapid reversible changes in dendritic spine structure in vivo gated by the degree of ischemia. J Neurosci 2005; 25: 5333–8.

Zhang S, Murphy TH. Imaging the impact of cortical microcirculation on synaptic structure and sensory-evoked hemodynamic responses in vivo. PLoS Biol 2007; 5: e119.

Zhao BQ, Wang S, Kim HY, Storrie H, Rosen BR, Mooney DJ, et al. Role of matrix metalloproteinases in delayed cortical responses after stroke. Nature Med 2006; 12: 441–5.

Zorner B, Filli L, Starkey ML, Gonzenbach R, Kasper H, Rothlisberger M, et al. Profiling locomotor recovery: comprehensive quantification of impairments after CNS damage in rodents. Nat Methods 2010; 7: 701–8.